AD-A232 610

REPORT DOCUMENTATION PAGE

Form Approved
OMB No. 0704-0188

1. AGENCY USE ONLY (Leave blank)	2. REPORT DATE	3. REPORT TYPE AND DATES COVERED
	15 November 1990	Final 16 April 1989- 30 Sept 1990

4. TITLE AND SUBTITLE
Chemical Reactions in Turbulent Mixing Flows

5. FUNDING NUMBERS
PE - 61102F
PR - 2308
TA - A2
G - 88-0155

6. AUTHOR(S)
Paul E. Dimotakis
James E. Broadwell
Anthony Leonard

7. PERFORMING ORGANIZATION NAME(S) AND ADDRESS(ES)
California Institute of Technology
Graduate Aeronautical Laboratories
Mail Stop 301-46
Pasadena, CA 91125

AFOSR-TR

8. PERFORMING ORGANIZATION REPORT NUMBER

9. SPONSORING/MONITORING AGENCY NAME(S) AND ADDRESS(ES)
AFOSR/NA
Building 410
Bolling AFB DC 20332-6448

10. SPONSORING/MONITORING AGENCY REPORT NUMBER

11. SUPPLEMENTARY NOTES

12a. DISTRIBUTION/AVAILABILITY STATEMENT
Approved for public release; distribution is unlimited

12b. DISTRIBUTION CODE

13. ABSTRACT (Maximum 200 words)

The purpose of this research has been to conduct fundamental investigations of turbulent mixing, chemical reaction and combustion processes in turbulent, subsonic and supersonic flows. This program is comprised of several efforts. In particular, an experimental effort, an analytical effort, a computational effort, a modeling effort, and a diagnostics development and data-acquisition effort; the latter as dictated by specific needs of the experimental part of the overall program. Our approach has been to carry out a series of detailed theoretical and experimental studies primarily in two, well-defined, fundamentally important flow fields: free shear layers and axisymmetric jets. To elucidate molecular transport effects, experiments and theory concern themselves with both liquids and gases, primarily in moderate to high Reynolds number flows. Modeling has been focused on both shear layers and turbulent jets, with an effort to include the physics of the molecular treansport processes, as well as formulations of models that permit the full chemical kinetics of the combustion process to be incorporated. Our recent analytical efforts have concentrated on a hydrodynamic analysis of the stability of compressible shear layers. The computational studies are, at present, focused at fundamental issues pertaining to the compurtational simulation of both compressible and incompressible flows.

14. SUBJECT TERMS	15. NUMBER OF PAGES
Turbulence, shear layers, jets, mixing, combustion, numerical simulation, light detection diagnostics, turbulent mixing modeling	47
	16. PRICE CODE

17. SECURITY CLASSIFICATION OF REPORT	18. SECURITY CLASSIFICATION OF THIS PAGE	19. SECURITY CLASSIFICATION OF ABSTRACT	20. LIMITATION OF ABSTRACT
Unclassified	Unclassified	Unclassified	UL

Abstract

The purpose of this research has been to conduct fundamental investigations of turbulent mixing, chemical reaction and combustion processes in turbulent, subsonic and supersonic flows. This program is comprised of several efforts. In particular,

a. an experimental effort,

b. an analytical effort,

c. a computational effort,

d. a modeling effort,

and

e. a diagnostics development and data-acquisition effort,

the latter as dictated by specific needs of the experimental part of the overall program.

Our approach has been to carry out a series of detailed theoretical and experimental studies primarily in two, well-defined, fundamentally important flow fields:

- free shear layers

and

- axisymmetric jets.

To elucidate molecular transport effects, experiments and theory concern themselves with both liquids and gases, primarily in moderate to high Reynolds number flows.

Modeling has been focused on both shear layers and turbulent jets, with an effort to include the physics of the molecular transport processes, as well as formulations of models that permit the full chemical kinetics of the combustion process to be incorporated.

Our recent analytical efforts have concentrated on a hydrodynamic analysis of the stability of compressible shear layers.

The computational studies are, at present, focused at fundamental issues pertaining to the computational simulation of both compressible and incompressible flows.

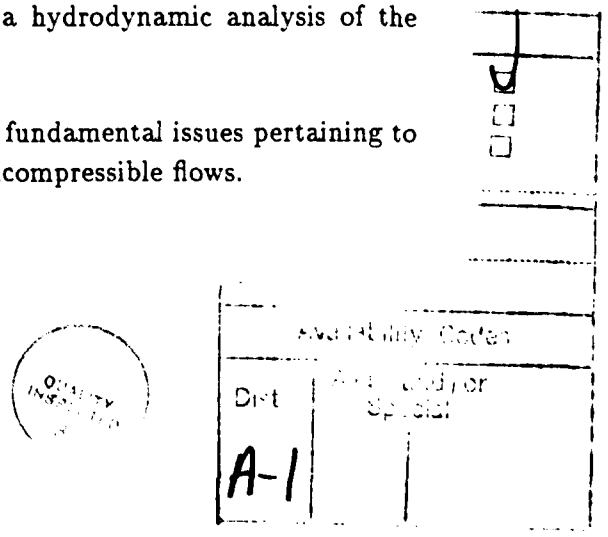

1. Introduction

Progress in the effort under the sponsorship of this Grant, for the period ending 15 April 1990, has been realized in several areas. In particular,

a. in supersonic shear layers, namely:

1. hydrodynamic linear stability analysis of homogeneous and inhomogeneous, compressible, bounded (confined) and unbounded free shear layers;

as well as

2. the completion of the supersonic shear layer facility

and the first

3. experimental investigations in non-reacting, supersonic shear layers[‡];

b. in the investigations of turbulent jets[♯], namely

1. investigations of gas phase, chemically reacting jets;
2. liquid phase jet mixing and interface topology studies;
3. large dynamic range investigations of the scalar dissipation (mixing rate) field;
4. the development of jet mixing models that permit the inclusion of full chemical kinetics calculations;

c. in the computational effort:

1. the development of lagrangian computational methods for compressible, unsteady flows that are inviscid or viscous, with or without chemical reactions and combustion;

and

2. the development of efficient algorithms for vortex dynamics calculations.

Finally, in our diagnostics effort,

d. we are proceeding with the next generation of data acquisition systems, as necessary to record the higher bandwidth signals generated by several experiments presently in progress.

These will be discussed below.

---

‡ The first reacting experiments have also been completed at this writing.

♯ The investigations of turbulent mixing and combustion in turbulent jets are co-sponsored by the Gas Research Institute.

2. Mixing and combustion in turbulent shear layers

The effort in turbulent mixing and combustion in high Reynolds number free shear layers is the largest part of this effort. This work will be summarized below.

2.1 Supersonic shear layer combustion facility

The first non-reacting experiments were in progress, at the end of the current reporting period, in the new GALCIT Supersonic Shear Layer Combustion Facility. These experiments come in the wake of the lower Reynolds number experiments of Papamoschou & Roshko (1988) and extend the range of flow parameters that can be investigated in many ways and, in addition, provide the capability of direct measurements of turbulent mixing through the use of fast chemical reactions. The flow here is a 2-D, compressible mixing layer, with either N_2 or He in the high speed stream and N_2 in the low speed stream. The free stream Mach numbers are $M_1 = 1.5$ and $M_2 = 0.3$ respectively. Some of the preliminary results are discussed below with the aid of three side-view Schlieren photographs.

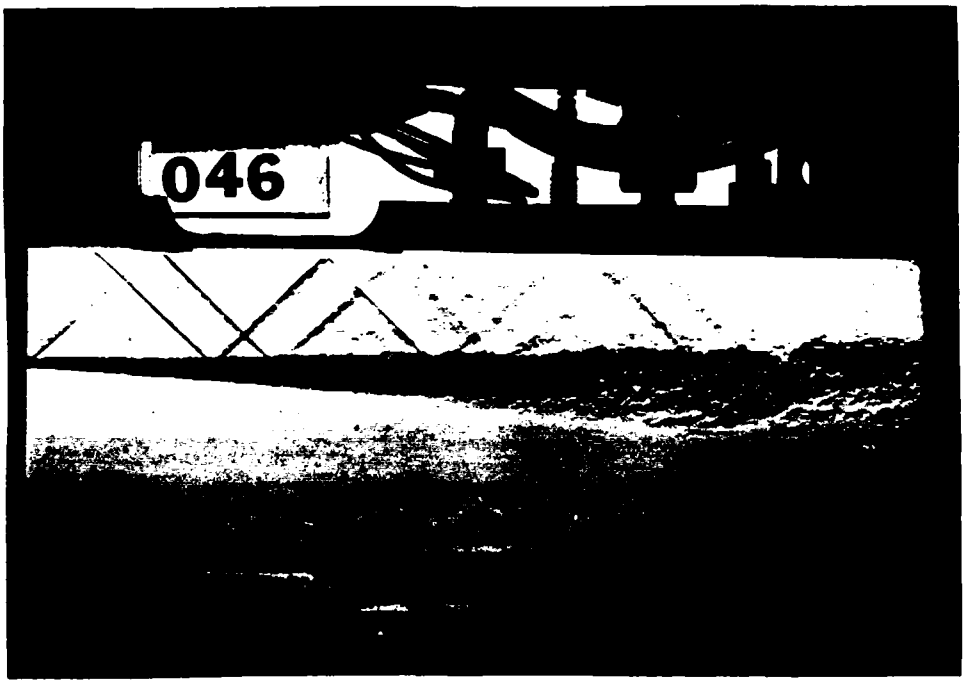

FIG. 1 Side view schlieren of $M_1 = 1.5$ N_2, $M_2 = 0.3$ N_2 pressure-matched, supersonic shear layer.

Figure 1 shows the basic form of the N_2/N_2 shear layer, with upper/lower guidewalls adjusted such that a negligible streamwise pressure gradient is imposed on the flow ($dp/dx \approx 0$). The shear layer is seen to form a well-defined, linearly growing wedge that appears devoid

of the two-dimensional coherent structures visible in incompressible shear layers. Similar observations were recently reported by Clemens *et al.* (1990) and Mungal & Clemens (1990).

Two standing waves are clearly visible in the supersonic stream. One originates from a small surface bump at the nozzle/top guidewall junction, while the second comes from the splitter tip. Both waves have been measured to be weak and can be seen to have little effect on the shear layer. They weaken further on subsequent reflections and gradually disappear downstream.

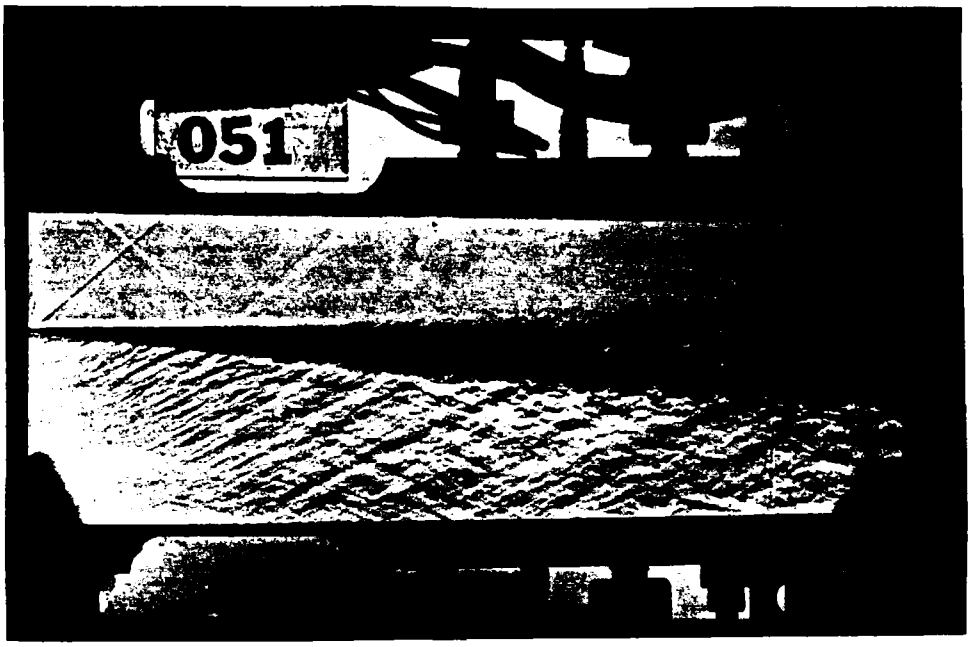

FIG. 2 Side view schlieren of $M_1 = 1.5$ N_2, $M_2 = 0.3$ N_2 overexpanded, supersonic shear layer.

Figure 2 shows a N_2/N_2 shear layer in which the supersonic stream is overexpanded, resulting in a strong oblique shock (compression) wave at the splitter tip. This wave, and its reflections, can be seen to result in considerable deflection of the shear layer. It is noteworthy, however, that the growth rate is basically unchanged from that of the unperturbed flow (*cf.* Fig. 1).

The third photograph (Fig. 3) is representative of the He/N_2 shear layers. Immediately obvious is the complex, yet regular, wave system in the low speed flow. This represents a system of travelling oblique shocks and expansion waves, probably created by (unseen) shear layer turbulent structures that appear large, *i.e.* comparable to the local shear layer thickness $\delta(x)$, and convect at speeds that are supersonic with respect to the low speed flow. The (convective) Mach number of these structures with respect to the low speed stream, as inferred from the angles of their associated waves, lies in the range of $2.0 \leq M_{c2} \leq 2.4$. This

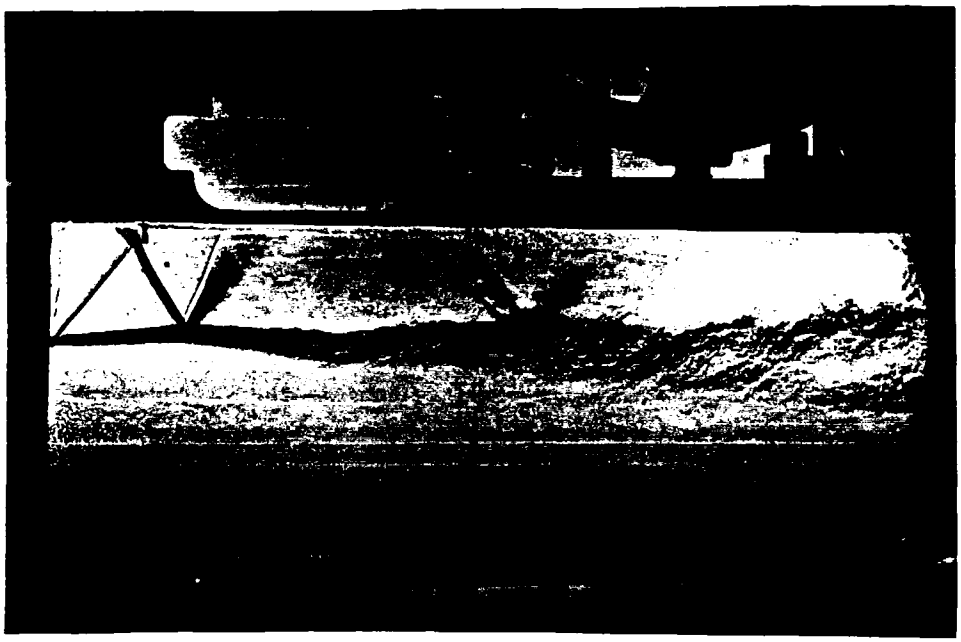

FIG. 3 Side view schlieren of $M_1 = 1.5$ He, $M_2 = 0.3$ N_2 pressure-matched, supersonic shear layer. Note oblique shock/expansion wave system in the low speed stream, generated by the supersonic turbulent structures in the layer.

should be compared to a value of the convective Mach number of $M_{c2}^{(i)} \approx 1.0$, based upon isentropic (shock-free) models of the convection velocity (*cf.* Papamoschou & Roshko 1988, Papamoschou 1989, Dimotakis 1989). These traveling waves are reminiscent of those seen in supersonic jet flows, *e.g.* Tam (1971), in which the waves originate from the supersonic shear layer in the vicinity of the jet exit. It should also be noted that the existence of these waves on only one side of the shear layer can be expected to be responsible for large effects on free stream fluid entrainment, with most of the growth occurring into the low speed side. It can also be inferred that, in this case, the convective Mach number with respect to the high speed stream is in the low *subsonic* range ($M_{c1} \simeq 0.3$).

At this writing, experiments performed have included the first direct investigations of entrainment, turbulent (molecular) mixing and chemical kinetics (Damköhler number) effects through the use of chemical reactions ranging from the slow to the fast kinetic limits. This part of the work will be documented in the upcoming reports and publications.

This effort is part of the Ph.D. research of Mr. Jeffery Hall, with the participation of Dr. Henning Rosemann, a Post Doctoral Research Fellow in Aeronautics.

2.2 Hydrodynamic instability of compressible shear layers

In support of the supersonic shear layer experiments, we have also been conducting linear stability analyses of compressible shear layers. During this last year, we have investigated the effect of upper/lower guidewalls on the stability of the flow. As had also been suggested by Tam & Hu (1989), we found (Zhuang *et al.* 1990, included in this report as Appendix A) that bounded shear layers are more unstable at high Mach numbers compared to unbounded shear layers, and that two-dimensional disturbances have greater amplification rates than the oblique waves that are found to be the more unstable in unbounded flow.

This effort is part of the Ph.D. research of M. Zhuang. A thesis (Zhuang 1990) documenting this part of the work has been completed, at this writing, and is available on application.

3. Mixing and combustion in turbulent jets

The research effort on turbulent jet mixing is cosponsored by the Gas Research Institute, GRI Grant No. 5087–260–1467.

3.1 Gas phase turbulent jet mixing

One of the major efforts expended as part of the overall program was the study of the behavior of the concentration field of the jet fluid in low to moderate Reynolds number ($5{,}000 \leq Re \leq 40{,}000$), gas phase, turbulent jets. To summarize, several important new conclusions stem from this part of the work and are briefly outlined below. The interested reader is referred to the detailed discussions in the publications cited below.

a. *All* measures of the mixing process in the far field ($x/d > 20$) become self-similar when scaled by the outer flow variables.

b. The mixing process is *not* found to be independent of the flow Reynolds number, as least in the range of Reynolds numbers investigated.

c. The local, instantaneous mixing rate spans *several decades**.

Additionally,

d. we also found evidence that the rate of *entrainment* by the jet of reservoir fluid is also Reynolds-number-dependent (at least for the gas phase flows and range of Reynolds numbers investigated).

This effort was conducted as part of the Ph.D. research of D. Dowling**. Available documentation of this work, at this writing, can be found in Dowling & Dimotakis (1988); the Dowling thesis (1988); Dowling, Lang & Dimotakis (1989) and, more recently, Dowling & Dimotakis (1990). One more publication is in preparation, at this writing, that should provide additional information and discussion of these results. Further investigations of consequences of these issues and ideas continue in work in progress in several contexts, as we will discuss below.

---

* See additional discussion and some new results in Sec. 3.4.

** Presently, Appl. Phys. Dept., U. Washington, Seattle.

3.2 Gas phase chemically reacting jet investigations

In work currently in progress, we are conducting an investigation of the Reynolds number effects on turbulent mixing and chemical product formation in turbulent jet diffusion flames. These experiments are conducted in the recently completed High Pressure Combustion Facility.

Considerable effort was expended during the previous year shaking down this new facility and developing the instrumentation and diagnostics. In the experiments in progress, the rate of chemical product formation and heat release is investigated by measuring the line integral of the temperature rise, in a direction transverse to the jet axis, in the range $30 \leq x/d \leq 240$. This measurement, described in the 1989 annual report (Dimotakis *et al.* 1989a, Sec. 3.1), is analogous to the product thickness used for the shear layer by Dimotakis (1989). Recall that the temperature measurement performed by each wire is the line integral at constant x given by

$$\frac{1}{L_w}\int_{L_w/2}^{L_w/2} \Delta T(x,y)\,dy \tag{1}$$

where L_w is the span (length) of the wire, x is the axial coordinate and y is the transverse coordinate. Here we will define the product thickness (δ_P), normalized by L_w as

$$\frac{\delta_P}{L_w} \equiv \frac{1}{L_w}\int_{-\infty}^{\infty} \frac{\Delta T(x,y)}{\Delta T_f}\,dy \tag{2}$$

where ΔT_f is the adiabatic flame temperature rise.

Early problems of recirculation within the tank were addressed by decreasing the jet nozzle diameter to 2.5 mm, reducing the extent of the flame zone and the time needed for reliable statistics to be extracted. The experiments currently in progress utilize the F_2/NO system with dilute reactants in N_2, a stoichiometric mixture ratio of $\phi = 12.14$ and a low adiabatic flame temperature of $\Delta T_f = 30.9\,K$ to mitigate buoyancy effects. Reynolds numbers that have been explored so far are in the range of $3{,}000 \leq Re \leq 100{,}000$. While these experiments must be considered preliminary, we see evidence of Reynolds number effects in the range of Reynolds numbers investigated. Specifically, our preliminary experiments suggest that for the range $20{,}000 \leq Re \leq 100{,}000$ the flame length, at fixed stoichiometric mixture ratio, is decreasing with increasing Reynolds number, albeit slowly.

Figure 4 shows the raw data from the 16 wires spanning $30 \leq x/d \leq 240$, along with two reference wires placed outside of the jet cone at $x/d = 0$ and $x/d = 240$, as well as the scaled velocity trace. The reference wire trace at $x/d = 240$ indicates the arrival of hot recirculated products at the last (highest) measuring station, thus establishing the temporal extent of the uncontaminated data record. The reference wire at $x/d = 0$ tracks the temperature of the ambient reservoir fluid and the scaled velocity trace marks the establishment of steady state flow. Note that $\Delta T_f \simeq 30.9\,K$ for this run.

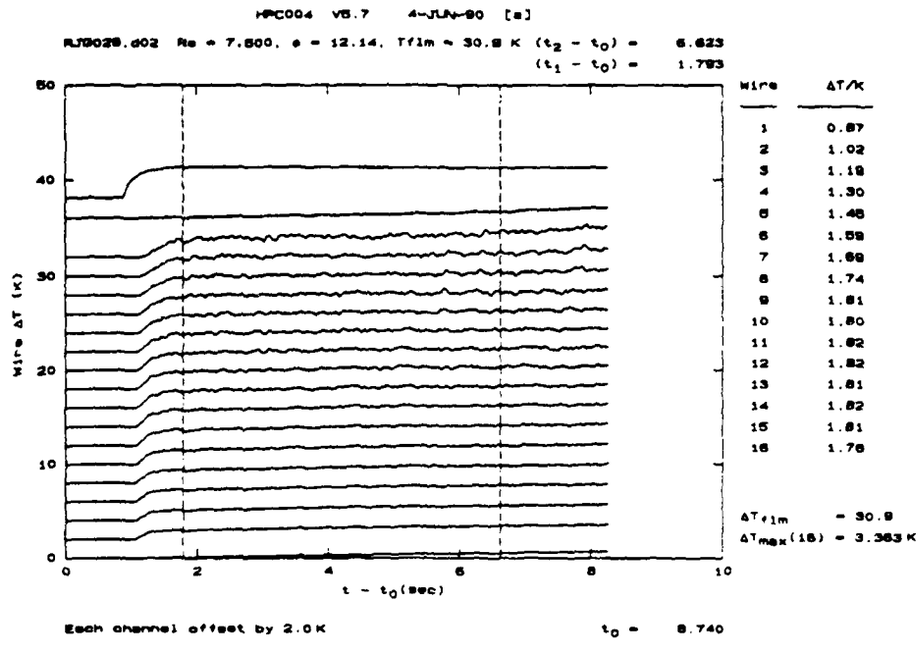

FIG. 4 Raw data traces of $L_w^{-1}\int \Delta T(x,y)\,dy$ for the 16 wires and 2 reference wires, along with a scaled velocity trace. The lower trace is the reference wire at $x/d = 0$ followed by the 16 measurements from $x/d = 30$ to 240, then the other reference wire at $x/d = 240$, and finally the scaled velocity trace.

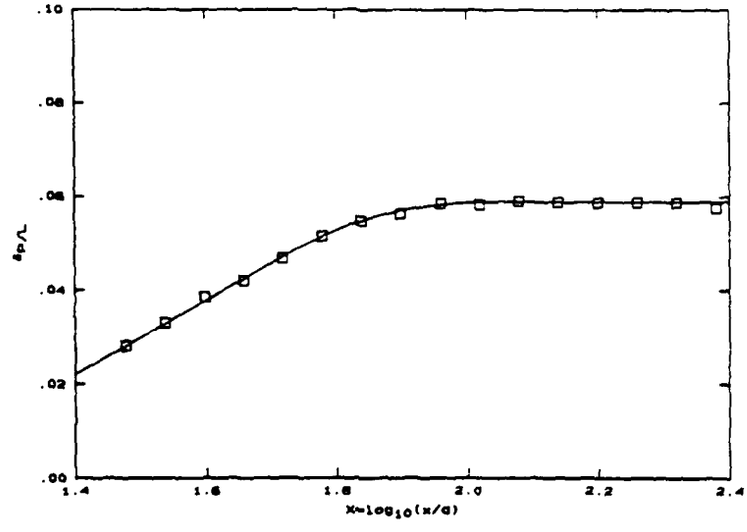

FIG. 5 Product thickness normalized by the wire length L_w calculated by dividing the time-averaged, line-integrated temperature rise from Fig. 4 by the adiabatic flame temperature ΔT_f.

These data were processed to produce Fig. 5, which shows the product thickness δ_P/L_w plotted versus $\log(x/d)$. The expected increase in the integrated temperature rise with x/d

can be seen, as well as the asymptotic value at the end of the flame tip. Plots like Fig. 5 for each Reynolds number are being used to identify any changes in the slope of the initial section, the location of the knee which can serve as a definition of flame length, as well as the final asymptotic temperature.

These experiments are part of the experimental effort of Richard Gilbrech.

3.3 Liquid phase turbulent jet mixing

We are continuing investigations of the fine scale turbulent structure in a liquid phase (high Schmidt number) axisymmetric jet. Laser-induced fluorescence concentration measurements have been taken at a range of Reynolds numbers from 3,000 to 24,000, both on the centerline and at several radial locations.

This work has yielded several interesting results to date. A study has been conducted to examine the applicability of a (power-law) fractal description to the geometry of the iso-scalar surfaces in the jet. As noted in our previous report, and as opposed to other studies, *e.g.* Sreenivasan & Meneveau (1986), we find that these surfaces *are not* locally characterized by a constant fractal dimension. We present a log-normal model of interface spacings that appears to capture the behavior of the experimental results.

A first paper discussing results from the study of the geometry of scalar interfaces was presented at the *ASME* La Jolla meeting in July 1989, and is to appear in the proceedings for that meeting (Miller & Dimotakis 1989). An abbreviated presentation covering these findings was later given at the *APS Fluid Dynamics Meeting* in Palo Alto (November 1989), and a much extended version of the work has been submitted to *Physics of Fluids*[†].

Another finding of this work concerns the behavior of the inertial range of the concentration power spectrum. It suggests the turbulence may, in some sense, not have reached its asymptotic behavior (as evidenced by an incipient, but underdeveloped, $-5/3$ slope) at a Reynolds number often considered to represent fully turbulent flow. In conjunction with the spectral findings, it is found that the normalized concentration RMS on the centerline of the jet *decreases with Reynolds number*. This is interpreted as further evidence that at Reynolds numbers in the range of 10,000 the jet has still not reached an asymptotic turbulent state, by some measures. This work was presented at an *IUTAM* conference in La Jolla, 20 August 1990 (Miller & Dimotakis 1990)[‡].

Lastly, the quality of the high Schmidt number concentration data has permitted us to compile statistics of the scalar dissipation. In conjunction with the gas phase data from

---

[†] To appear, *Phys. Fluids A*, Jan 1991.

[‡] Submitted for publication to the *Phys. Fluids A*.

Dowling (1988), this allows us to examine Schmidt number effects in turbulent jet mixing. Progress to date includes the derivation of an analytic method for the recovery of the three-dimensional scalar dissipation PDF from the measured one-dimensional PDF, given an assumption of local, small-scale isotropy. This will be discussed in some detail in Sec. 3.4 below.

Plans for the future include use of the Photometrics camera system (see Sec. 5.2 below) to examine a host of interesting problems in the turbulent jet. Also, 'second generation' single point measurements will be made, extending our previous capabilities in resolution, signal-to-noise, and Reynolds number. These should permit more extensive investigations of the issues discussed above.

This work is part of the Ph.D. research of Paul Miller.

3.4 Molecular mixing rate. Scalar dissipation.

It has been proposed that the stochastic behavior of the dissipation of the local kinetic energy per unit mass, *i.e.*

$$\varepsilon(\mathbf{x},t) \;=\; \frac{\nu}{2}\sum_{i,j}\left(\frac{\partial u_i}{\partial x_j}+\frac{\partial u_j}{\partial x_i}\right)^2 \;, \tag{3}$$

in high Reynolds number, fully developed turbulence should be describable by log-normal statistics (Kolmogorov 1962, Oboukhov 1962, Gurvich & Yaglom 1967). See also Monin & Yaglom (1975, p. 585) for a discussion and additional references. The arguments that lead to this conclusion are rather broad and basically rely on the assumption that the generating process for the quantity of interest relies, in turn, on successive fractionations of the associated scales to produce the resulting statistical equilibrium; an appealing description of the turbulent cascade process (Kolmogorov 1941). In particular, this argument would suggest that the same conclusion should apply to the local *scalar* dissipation rate,

$$\zeta(\mathbf{x},t) \;=\; 2\mathcal{D}\,\chi(\mathbf{x},t) \;, \tag{4}$$

i.e. the square $[c(\mathbf{x},t)-\bar{c}\,]^2$ of the fluctuations of the scalar field $c(\mathbf{x},t)$ about its local mean $\bar{c}$, where

$$\chi(\mathbf{x},t) \;\equiv\; \left|\frac{\partial c}{\partial \mathbf{x}}\right|^2 \;=\; \left(\frac{\partial c}{\partial x}\right)^2+\left(\frac{\partial c}{\partial y}\right)^2+\left(\frac{\partial c}{\partial z}\right)^2 \;. \tag{5a}$$

and $\mathcal{D}$ is the appropriate molecular diffusivity coefficient, as it appears in the transport equation for the scalar field $c(\mathbf{x},t)$, *i.e.*

$$\frac{\partial c}{\partial t}+\mathbf{u}\cdot\frac{\partial c}{\partial \mathbf{x}} \;=\; \mathcal{D}\nabla^2 c \;. \tag{6}$$

This is an important observation in the context of turbulent mixing, chemical reactions and combustion. The local scalar dissipation $\zeta(\mathbf{x},t)$ measures the local rate of mixing (molecular diffusion) and can be related directly to the local chemical reaction rate, in the limit of infinite kinetics (Bilger 1979). It therefore bounds the rate of local chemical reaction that can be realized at $(\mathbf{x},t)$. From a modeling vantage point, the statistics of $\chi(\mathbf{x},t)$, and therefore $\zeta(\mathbf{x},t)$, ultimately describe the mixing rates that are handed to the chemical kinetics by the turbulent mixing process and determine the extent to which the chemistry in the flow/combustion system can be regarded as kinetically fast or slow.

Subsequently to the original proposals, investigators have implied that, at least for an isotropic field, the statistics of quantities such as $(\partial u/\partial x)^2$, the square of the partial derivative of the streamwise velocity component along the streamwise direction, which is one of the terms comprising the local energy dissipation (Eq. 3), should also obey log-normal statistics. Arguments are then given to explain the departures of the measured histogram (PDF) of values from log-normality, with the observations suggesting an excess of probability at low values of $(\partial u/\partial x)^2$ and a defect at high values, relative to the log-normal distribution (see discussion and references in Monin & Yaglom 1975, pp. 635–637).

If these same arguments were to be applied to scalar dissipation they would involve the statistics of the square of one component of the gradient of the scalar field, say,

$$\chi_1(\mathbf{x},t) \equiv \left(\frac{\partial c}{\partial x}\right)^2 , \tag{5b}$$

and would assert that $\chi_1(\mathbf{x},t)$ should also display log-normal statistics. The assertion, however, is false, as the statistics of χ_1 are, in fact, different from the statistics of χ. This can be illustrated by the argument below.

It is easy to show that small values of $\chi_1(\mathbf{x},t)$ are rather more likely than small values of $\chi(\mathbf{x},t)$. The latter require that *all three* components of the scalar gradient must be small at the same $(\mathbf{x},t)$. See, for example, discussion in Dowling (1988)[‡].

This issue of whether the statistics of $\chi = |\nabla c|^2$ can be inferred from the statistics of $\chi_1 = (\partial c/\partial x)^2$ is an important one to resolve because direct measurements of the 3-D gradient, and therefore the scalar dissipation ζ are difficult under any circumstances. In particular, they are typically out of reach in flows with the moderate to high Reynolds numbers of interest in the present context, in view of the spatial/temporal resolution and signal-to-noise requirements at these flow conditions. On the other hand, the statistics of $\chi_1 = (\partial c/\partial x)^2$ are easier to estimate experimentally, using the approximation

$$\chi_1 = \left(\frac{\partial c}{\partial x}\right)^2 \approx \frac{1}{\bar{u}^2}\left(\frac{\partial c}{\partial t}\right)^2 , \tag{7}$$

[‡] We note here that similar objections can also be raised concerning the statistics of $(\partial u/\partial x)^2$ *vs.* the statistics of the norm of the symmetric part of the velocity gradient tensor, which enters in the expression for the local energy dissipation (Eq. 3).

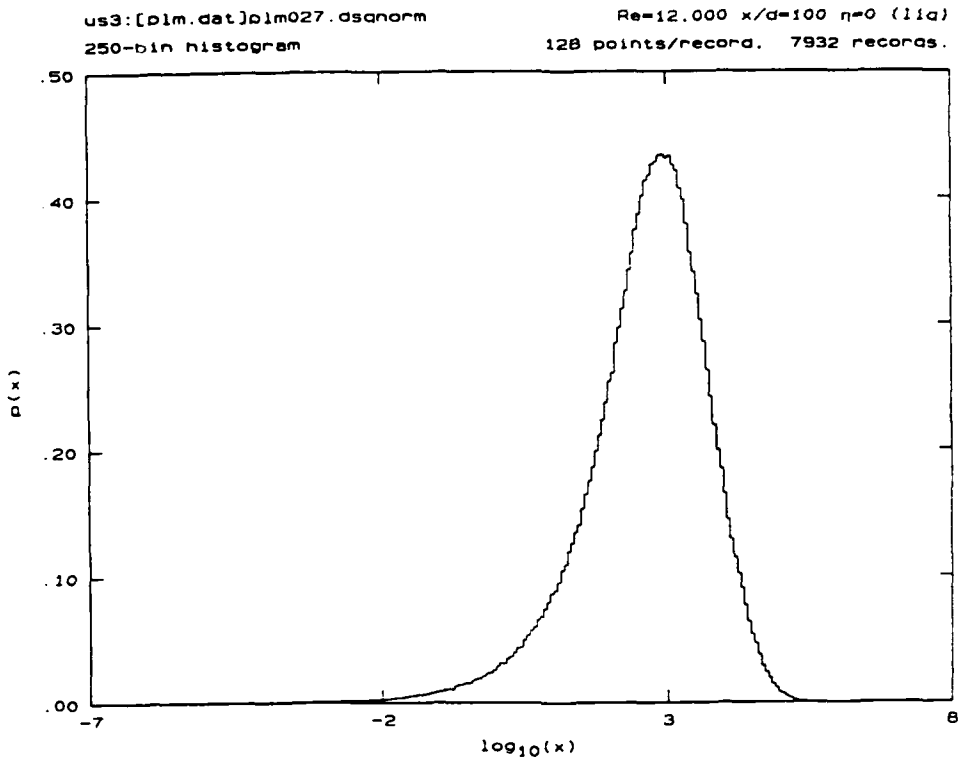

FIG. 6a PDF of χ_1, in arbitrary units, measured on the axis ($r/x = 0$) of a liquid turbulent jet, at a Reynolds number of $Re = 12{,}000$, at $x/d = 100$ (unpublished data by Miller & Dimotakis).

which is usually adequate for extracting the statistics of χ_1, provided the fluctuations in $u/\bar{u}$ are not too large, where $\bar{u}$ is the local mean of the streamwise velocity. See related discussion in Dimotakis, Broadwell & Zukoski (1989c, pp. 2–3).

An implicit numerical reconstruction method for estimating $p(\chi)$ from the measured $p_1(\chi_1)$ was recently put forth by Dahm & Buch (1989), who, on the basis of the first few moments of the reconstructed PDF of χ of some of Dowling's (1988) data, concluded that the first few moments of the PDF of $\log_{10}\chi$ were close to those of a gaussian*. As we will show below, however, it is possible to carry out the inversion analytically and make an even

* A minor error in implementing the results of that inversion led to the conclusion that $\langle\chi\rangle$, the expectation value of χ, was almost 7 times higher than $\langle\chi_1\rangle$, the expectation value of χ_1. For an isotropic field, however, we must have

$$\langle\chi\rangle = 3\langle\chi_1\rangle. \tag{8}$$

In particular, the moment of $\log_{10}\chi$ was computed, rather than the logarithm of the moment (Dahm, private communication). Nevertheless, the numerical inversion of Dahm & Buch appears to be basically correct. The conclusion that at least the first few moments of the scalar dissipation are in accord with log-normal statistics is an important one.

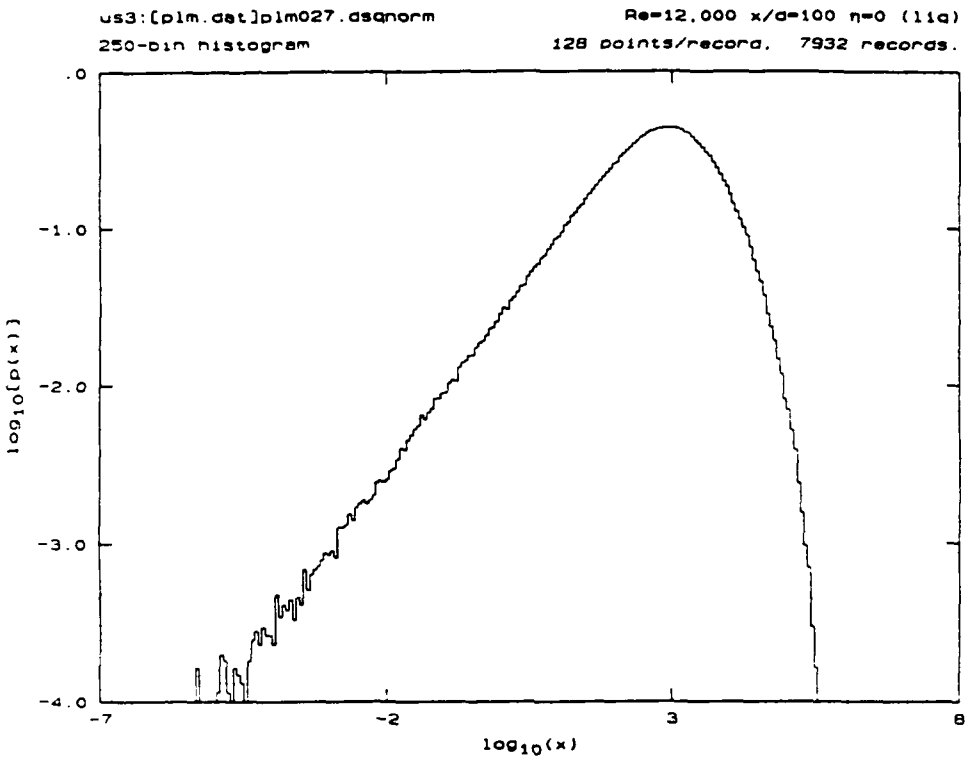

FIG. 6b Logarithm (base 10) of PDF of χ_1, in arbitrary units. Same data as in Fig. 6a.

stronger identification of the statistics of the scalar dissipation.

We begin by examining the data. By way of example, Fig. 6a is a plot of the probability density function (PDF) of χ_1, in arbitrary units, measured on the axis ($r/x = 0$) of a liquid turbulent jet, at a Reynolds number of $Re \simeq 12{,}000$, at $x/d = 100$ (unpublished data by Miller & Dimotakis). The same data are depicted in Fig. 6b, which plots the (decimal) logarithm of the same PDF. We appreciate that, if the statistics of χ_1 were log-normal, the resulting curve would have been an (inverted) parabola. Note the very large range of values of the measured quantity, almost 10 decades in χ_1 (*i.e.* 5 decades in $|\partial c/\partial t|$), and the behavior

$$\ln P_1(\ln \chi_1) \sim \text{const.} + \frac{1}{2} \ln \chi_1 \ , \tag{9a}$$

for small values of $\ln \chi_1$, which yields, for the PDF of χ_1,

$$p_1(\chi_1)\, d\chi_1 \propto \frac{d\chi_1}{\sqrt{\chi_1}} \tag{9b}$$

for small values of χ_1. Similar data and conclusions were first presented in Dowling (1988) for gas phase jets at comparable Reynolds numbers and were reported previously.

To discuss this issue, consider the vector space spanned by ∇c, the local gradient of $c(\mathbf{x},t)$, with coordinates (c_1,c_2,c_3), *i.e.*

$$\nabla c \;=\; \frac{\partial c}{\partial \mathbf{x}} \;=\; \left[\frac{\partial c}{\partial x_1},\, \frac{\partial c}{\partial x_2},\, \frac{\partial c}{\partial x_3}\right]^{\mathrm{T}} \;\equiv\; [c_1,c_2,c_3]^{\mathrm{T}} \;. \tag{10}$$

See Fig. 7. Note that, by construction,

$$\chi_1 \;=\; c_1^2 \;=\; \chi\cos^2\theta \;, \tag{11}$$

where θ is the angle subtended between ∇c and the c_1-axis.

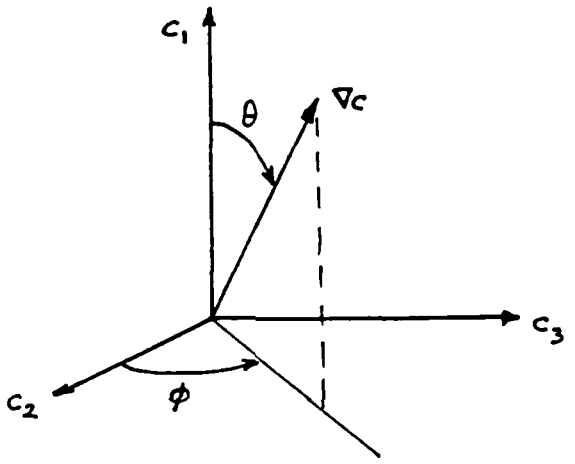

FIG. 7 Coordinate space of ∇c. Measured component along c_1-axis.

If $p_1(\chi_1)$ is the known (measured) PDF of χ_1 and $p_2(\chi_1,\chi)$ is the joint PDF of χ_1 and χ, the (full) gradient squared (Eq. 5a), we must have**

$$p_1(\chi_1) \;=\; \int_{\chi_1}^{\infty} p_2(\chi_1,\chi)\,d\chi \;=\; \int_{\chi_1}^{\infty} p_c(\chi_1|\chi)\,p(\chi)\,d\chi \;, \tag{12a}$$

where $p(\chi)$ is the (desired) PDF of χ and $p_c(\chi_1|\chi)$ is the *conditional* PDF of χ_1, given χ. The latter must be normalized such that

$$\int_0^{\chi} p_c(\chi_1|\chi)\,d\chi_1 \;=\; 1 \;. \tag{12b}$$

Now $p_c(\chi_1|\chi)$ represents the probability density that the angle θ, subtended between ∇c and the c_1-axis, is in the correct interval $(\theta,\, \theta+d\theta)$. In 3-D, this translates to

$$p_c(\chi_1|\chi)\,d\chi_1 \;=\; f\,[\Omega(\theta,\phi)]\;d\Omega \;,$$

** Note that *given* χ_1, $\min\{\chi\} = \chi_1$.

where $d\Omega$ is the differential solid angle containing the direction of ∇c, and $f(\Omega)$ is the PDF of Ω. For an isotropic ∇c-field, $f(\Omega)$ must be a constant and we must have (recall that $\chi_1 = \chi \cos^2\theta$)

$$p_c(\chi_1|\chi)\,d\chi_1 \;=\; 2\,p_c(\chi_1|\chi)\,\chi\,|\sin\theta\,\cos\theta|\;d\theta \;\propto\; d\Omega \;\propto\; |\sin\theta|\,d\theta\;,$$

or,

$$p_c(\chi_1|\chi) \;\propto\; \frac{1}{\chi\,|\cos\theta|} \;=\; \frac{1}{\chi\sqrt{\chi_1/\chi}}$$

and therefore

$$p_c(\chi_1|\chi) \;=\; \begin{cases} \dfrac{1}{2\sqrt{\chi\,\chi_1}}\;, & \text{for } \chi_1 \le \chi\;; \\ 0\;, & \text{otherwise,} \end{cases}$$

where the normalization factor has been determined using Eq. 12b. Substituting in the relation between $p_1(\chi_1)$ and $p(\chi)$ of Eq. 12, we obtain the desired result. In particular, for an isotropic ∇c-field in 3-D, we have

$$p_1(\chi_1) \;=\; \frac{1}{2\sqrt{\chi_1}}\int_{\chi_1}^{\infty} p(\chi)\,\frac{d\chi}{\sqrt{\chi}}\;, \tag{13}$$

which can also be inverted to express $p(\chi)$, the PDF of χ, in terms of $p_1(\chi_1)$, the measured PDF of χ_1, *i.e.*

$$p(\chi) \;=\; -2\sqrt{\chi}\,\frac{d}{d\chi}\left[\sqrt{\chi}\,p_1(\chi)\right]\;. \tag{14}$$

Note that, provided $p(\chi)$ is not too large as $\chi \to 0$, the resulting expression (Eq. 13) for $p_1(\chi_1)$ possesses the asymptotic behavior noted in Eq. 9b, as $\chi_1 \to 0$. Analogous expressions can be obtained to invert measurements of one component of a 2-D scalar gradient, for an isotropic ∇c-field in 2-D.

To test for log-normality we could apply Eq. 14 directly to compute the desired $p(\chi)$ from the measured $p_1(\chi_1)$. This would, effectively, entail differentiating the curves in Fig. 6a, to see if the resulting $p(\chi)$ is log-normal. It is preferable, however, to compute the expected $p_1(\chi_1)$, *assuming* that $p(\chi)$ is log-normal, and then test whether the resulting PDF provides a good fit to the measured $p_1(\chi_1)$. This avoids the unpleasantness of differentiating data.

It facilitates the calculations to transform the problem to logarithmic variables. To this end, ξ and ξ_1 are defined such that

$$\xi \;\equiv\; \ln\chi \qquad \text{and} \qquad \xi_1 \;\equiv\; \ln\chi_1\;.$$

In these coordinates, the relation of Eq. 13 between $p_1(\chi_1)$ and $p(\chi)$ becomes

$$P_1(\xi_1) \;=\; \frac{e^{\xi_1/2}}{2}\int_{\xi_1}^{\infty} e^{-\xi/2}\,P(\xi)\,d\xi\;, \tag{15}$$

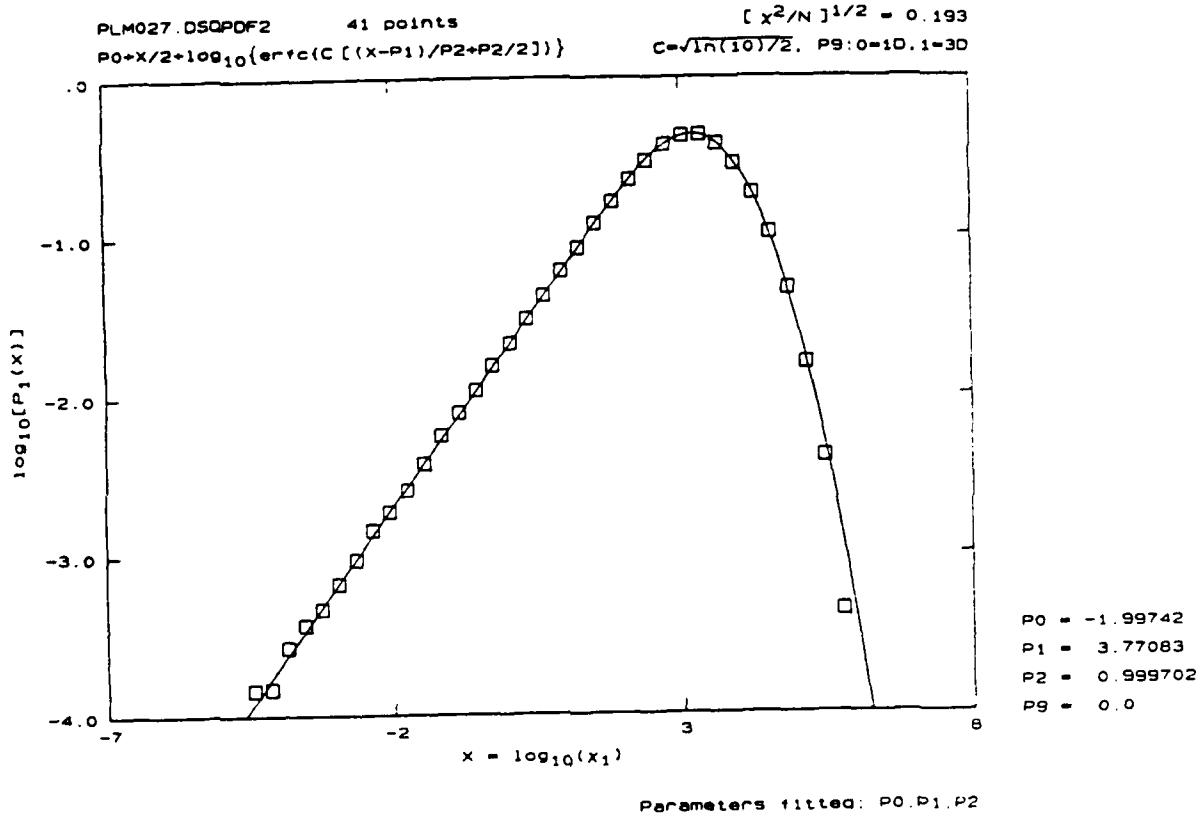

FIG. 8a Least squares fit to the data in Fig. 6b, assuming log-normal statistics for the scalar dissipation.

where $P_1(\xi_1)\,d\xi_1$ is the PDF of ξ_1 and $P(\xi)\,d\xi$ is the PDF of ξ. A log-normally distributed $\chi = |\nabla c|^2$ corresponds to a PDF of the $\xi = \ln\chi$ coordinate given by a gaussian, *i.e.*

$$P(\xi) \propto \exp\left\{ -\frac{1}{2}\left(\frac{\xi - \xi_0}{\sigma}\right)^2 \right\} , \tag{16}$$

in which ξ_0 and σ are the mean and variance of the $\xi = \ln\chi$ distribution. Substituting this in Eq. 15 then yields

$$P_1(\xi_1) \propto e^{\xi_1/2}\,\mathrm{erfc}\left\{ \frac{1}{\sqrt{2}}\left(\frac{\xi_1 - \xi_0}{\sigma} + \sigma\right) \right\} , \tag{17}$$

where $\mathrm{erfc}(x)$ is the complementary error function. Note that the resulting $P_1(\xi_1)$ is a function of *two* parameters, the mean ξ_0 and the variance σ^2. The third (implicit) constant of proportionality in Eq. 17 is determined by the normalization condition on $P_1(\xi_1)$.

Does this provide a good fit to the data?

Figure 8a plots the resulting least squares fit to the PDF of χ_1. The data are those in Fig. 6b, recomputed as a histogram with a smaller number of bins to facilitate the fit.

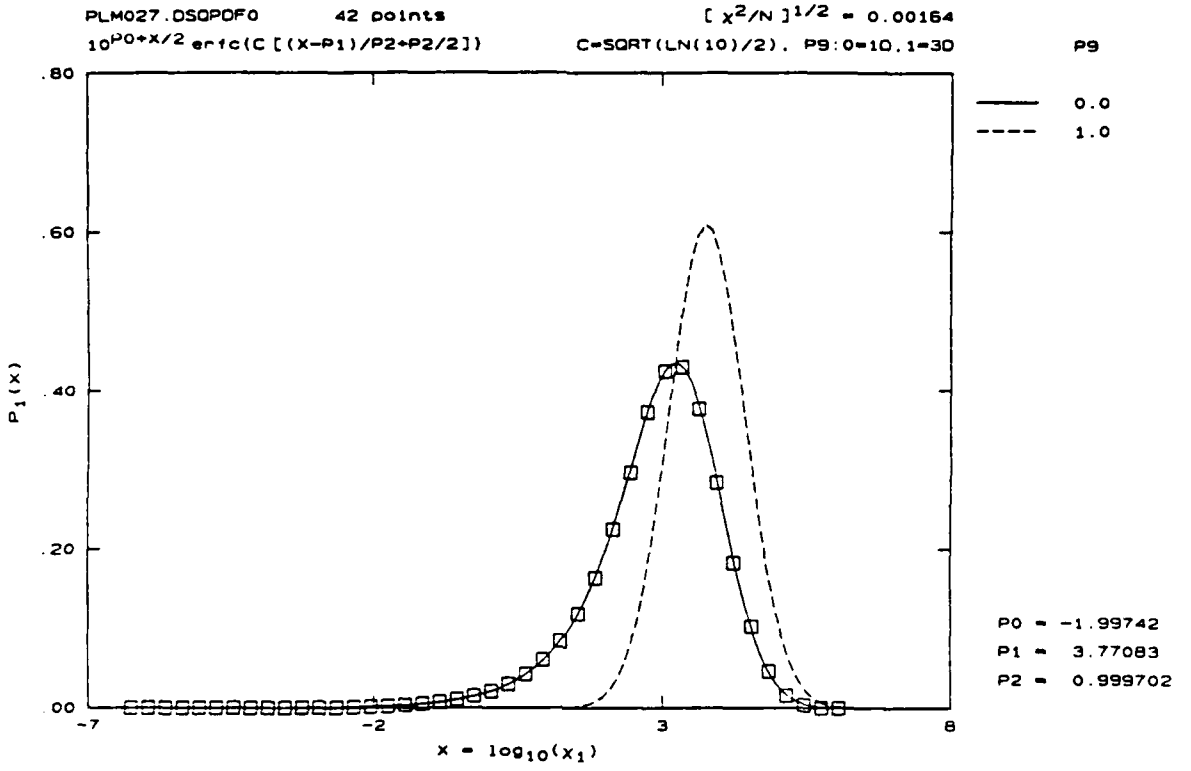

FIG. 8b Fit (solid line) to $P_1(\log_{10}\chi_1)$ (Fig. 6a). Dashed line represents the gaussian PDF of the (decimal) logarithm of the 3-D $\chi = |\nabla c|^2$.

It can be seen that, except for the largest values of ξ_1, the analytical expression of Eq. 17 provides an excellent two-parameter fit, *over the many decades spanned by the data for* χ_1. Figure 8b plots the fit (solid line) in linear PDF axis coordinates (cf Fig. 6a), as well as the gaussian PDF of the 3-D $\chi = |\nabla c|^2$ (dashed line). Similar results are obtained with the scalar dissipation gas phase data of Dowling (1988). See Fig. 9.

Several important conclusions can be drawn from these results.

a. Except for the highest values that can be realized, the local scalar dissipation appears to conform exceptionally well to log-normal statistics. At this point, it is not clear whether this is attributable to

   i. limitations in the dynamic range of the measurements, which effectively truncate the highest values from the true distribution;

   ii. a failure of isotropy for events yielding the highest values;

   or,

   iii. a failure of the log-normal hypothesis at these values.

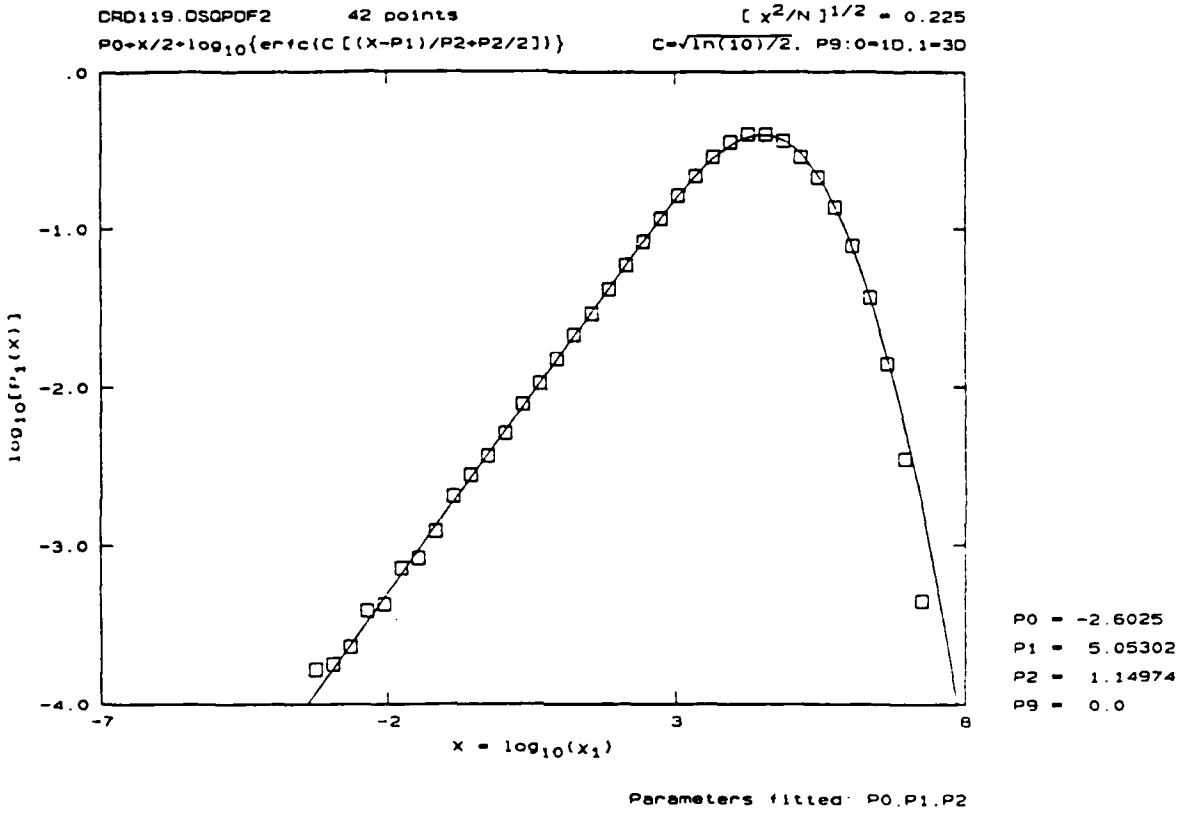

FIG. 9 Least squares fit to the gas phase, $Re = 16{,}000$, on-axis data of Dowling (1988).

b. This is *not* the case for the statistics of the square of any one component of the scalar gradient.

c. The local molecular mixing (diffusion) rate, as measured by the scalar dissipation $\zeta(\mathbf{x},t) = 2\mathcal{D}\,|\nabla c|^2$, varies over a range in excess of *3 orders of magnitude*. This implies that one cannot use a single mixing rate in describing the turbulent mixing to the chemical kinetics, at least for moderate to high Reynolds number turbulent jets.

We should close by noting that the Kolmogorov/Oboukhov log-normal proposals for the *energy* dissipation rate also deal with the dependence of the variance on such flow parameters as the Reynolds number. In the case of *scalar* dissipation (mixing), however, the variance σ, which measures the range of values of $\zeta(\mathbf{x},t)$ that are encountered, is expected to depend on both the flow Reynolds number as well as $Sc \equiv \nu/\mathcal{D}$, the fluid Schmidt number. We propose to study this important dependence, both experimentally and theoretically, as part of our research effort in the near future.

A first report of these results was made at the 42nd *APS/DFD Annual Meeting* (Palo Alto, California), 19–21 November 1989 (Dimotakis *et al.* 1989b).

3.5 Joint Caltech–Sandia National Laboratories Modeling Effort

A major modeling effort supported in part by the present contract has been the development of a model for chemical reactions in a turbulent fuel jet that is based upon the ideas first put forward by Broadwell & Breidenthal (1982) for the shear layer. A refinement and clarification of these ideas is described in Broadwell & Mungal (1988) where again the application is to reactions in a shear layer, in particular, to the $H_2 - F_2 - NO$ reaction studied experimentally by Mungal & Dimotakis (1984) and Mungal & Frieler (1987).

The initial steps in the formulation of the jet model are described in Broadwell (1987), and the continuing work is as outlined there. Briefly, the entrained air is envisioned to enter the fuel jet in large-scale streams where it initially forms strained diffusion layers or flame-sheets together with the local product and unburned fuel stream. As these layers lengthen, they are drawn together and eventually merge to form what is taken to be a mixture of uniform or homogeneous composition, *i.e.* to be in a perfectly stirred reactor. Supporting evidence for this picture of turbulent mixing is emerging from several experiments: Dahm & Buch (1989b), Mungal & Hollingsworth (1989), Seitzman *et al.* (1990), and Papantoniou & List (1989).

In collaboration with personnel of the Sandia National Laboratories — A. E. Lutz, R. J. Kee, and R. W. Dibble (now at University of California, Berkeley), this picture of molecular mixing and chemical reaction is being put in the form of a numerical model. The following is a discussion of initial work on this task and represents a preliminary interpretation made together with the above named group.

As an interim measure, a simpler version of the model in which the strained flame reactions are also assumed to be described by a perfectly-stirred reactor has been formulated and applied to hydrogen and propane flames burning in air. Preliminary comparisons have also been made with the initial Caltech $NO - F_2$ experimental results, but a thorough comparative study will be made when more results are available. A schematic of the "two-reactor" model is shown in Figure 10.

The air flux in the model is set by the molecular mixing rate inferred from the experiments of Weddell (1941) and Dahm & Dimotakis (1987) while the return flux from the homogeneous reactor is such as to maintain the flame-sheet reactor at the stoichiometric mixture ratio (to simulate the flame-sheet condition.)

Recent experiments by Barlow *et al.* (1990) in a turbulent nonpremixed jet flame, in which the fuel is a mixture of 22% argon in hydrogen, provide a significant test of the model. The fuel a mixture that retains the simplicity of the hydrogen chemical kinetics. The experiment applies simultaneously laser-Raman scattering, which measures the mixture fraction f, and laser-induced fluorescence, which measures the concentration of an important intermediate species, the hydroxyl radical OH.

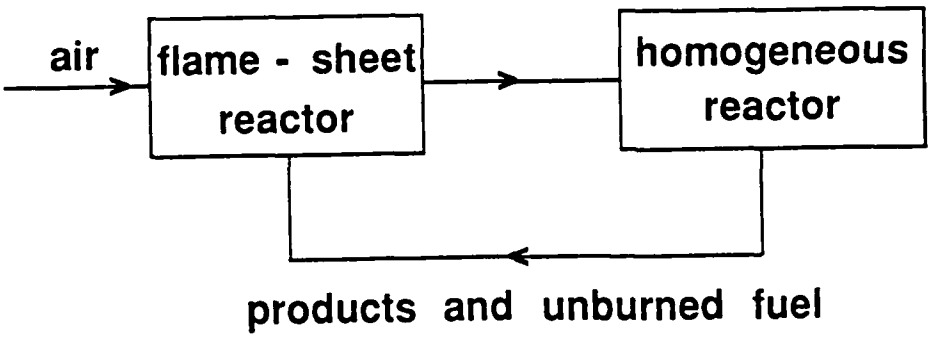

FIG. 10 Schematic of "Two-reactor" model.

For the conditions of Barlow *et al.* (1990), computations have been made at Sandia of the axial evolution of the chemical species in the two reactors for the two jet velocities, 75 and 150 m/s. Figure 11 shows the predicted OH mole fractions and fuel mixture fractions, f, as functions of distance from the nozzle. The laser-based measurements are reported for two axial locations, $x/d_0 = 30$ and $x/d_0 = 50$. For comparison with the model results, we select $f - \mathrm{OH}$ pairs in which f is within 5% of the stoichiometric value, 0.16. The average of these conditioned pairs is shown in Fig. 11 as single points, where the agreement with the model is seen to be good. The mixture fraction is nearly the same in the two reactors at $x/d_0 = 50$, which is nearly the flame length. The agreement aside, it is important to note that both the prediction and measurement are substantially above the stoichiometric equilibrium mole fraction of 0.005, and that, therefore, the model captures this essential feature for reaction with simultaneous mixing.

Turns & Lovett (1989) recently measured $\mathrm{NO_x}$ in the combustion products from a propane flame attached to a 3.8 mm. diameter nozzle with jet velocities ranging from 35 m/s to 69 m/s. We model this flame using a propane-air oxidation mechanism (259 reactions and 55 species) derived from Westbrook & Pitz (1984) and incorporating the nitrogen chemistry from Miller & Bowman (1990). Figure 12 shows the axial development of composition of the two reactors. For the first 50 diameters, NO steadily increases in both reactors due solely to production in the flame reactor. Surprisingly, a significant *decrease* in NO occurs at approximately 120 diameters. This decrease is caused by fuel-rich reactions in the homogeneous reactor that remove NO[†]. As the homogeneous reaction evolves from

[†] NO removal in fuel-rich combustion is the basis of staging/reburning for NO control in power plants.

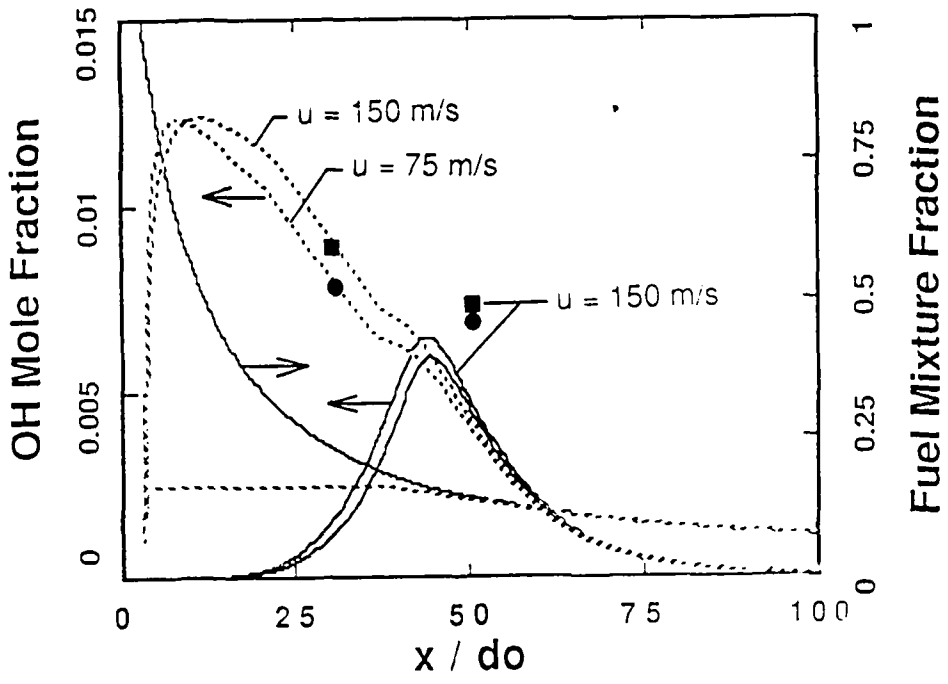

FIG. 11 Predicted mixture fraction and OH mole fraction profiles for the H_2/Ar flame of Barlow *et al.* (1990) at two jet velocities. Also shown are measured OH mole fractions at 30 and 50 diameters; squares represent u_0 = 75 m/s; circles represent u_0 = 150 m/s. Solid curves represent the homogeneous reactor and dashed curves represent the flame-sheet reactor. The mixture fraction solution is independent of velocity. Computations shown in Figs. 11, 12, and 13 were made at Sandia National Labs.

fuel-rich chemistry to fuel-lean chemistry at the flame tip, the NO in the homogeneous reactor rapidly increases. Because of the fuel-rich NO_x removal reactions, most of the NO_x in the combustion products is generated near the flame tip in the "last reactive eddy." Consequently, modifications to the flame near the nozzle have little impact on the total NO_x if these modifications do not change the residence time in the flame tip region. A point on which the model fails to agree with the experiment is in the ratio NO_2/NO_x. The experimental values are as high as 40%, while the model predicts negligible NO_2. This important difference is yet unexplained and is presently being studied.

Beyond the flame tip (Fig. 12) the NO_x concentration decreases primarily due to dilution of entrained air. These dilution effects are separated from the chemical kinetic effects by normalizing the NO_x concentration with mixture fraction, which is a direct measure of air dilution throughout the flame. An often-used normalized variable, called the emission index, E, is the mass flux of NO_x, per unit mass flux of fuel. As expected, we predict that well beyond the flame tip the emission index is constant.

The conventional expectation (as discussed, for example, by Bilger & Beck 1988 and Peters & Donnerhack 1981), is that E increase linearly with flame residence time, τ_0 =

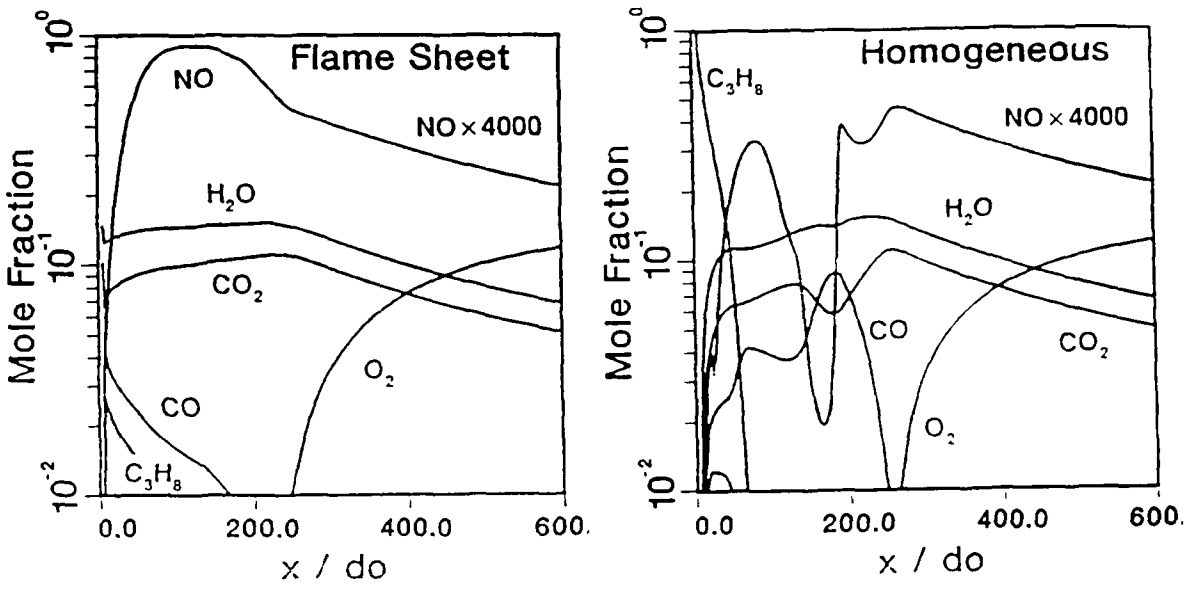

FIG. 12 Computed species mole fractions in the two reactors for a propane jet: $u_0 = 69\,\mathrm{m/s}$, $d_0 = 0.386\,\mathrm{cm}$. Beyond the flame tip (≈ 200 diameters), the concentration of the product species decreases due to entrainment and dilution. NO is first produced in the flame-sheet reactor, but roughly half of this NO is destroyed in the homogeneous reactor.

d_0/u_0. Contrary to this expectation, Turns and Lovett find that NO_x increases as τ_0 decreases. Turns proposes that his results can be explained by thermal radiation losses and our model supports this view. In our relatively simple radiation model, we chose a constant $\epsilon = 0.1$ to match the measured E at $u_0 = 69\,\mathrm{m/s}$. Then, as seen in Fig. 13, we predict the observed trend (but with a somewhat different slope).

When we neglect thermal radiation, we find that E/τ_0 decreases as τ_0 increases, and the predicted emission index is more than 10 times larger than measured. Including radiation results in a reduction of flame-tip temperature from 2270 K to 1970 K. It is apparent from these results that proper accounting of radiation is central to our understanding of nitric oxides emissions from turbulent flames. Tyson *et al.* (1990) reached similar conclusions in a study using an analogous implementation of the ideas discussed above.

We emphasize that the entrainment and mixing rules used here are appropriate to momentum-dominated jets. The H_2/Ar experiments that we refer to are momentum dominated, whereas the propane experiments clearly have buoyancy effects that modify the entrainment and mixing rates. However, the structure of the model is such that it can readily accommodate buoyancy effects, such as those described by Becker & Yamazaki (1978), and such effects will be incorporated in future work.

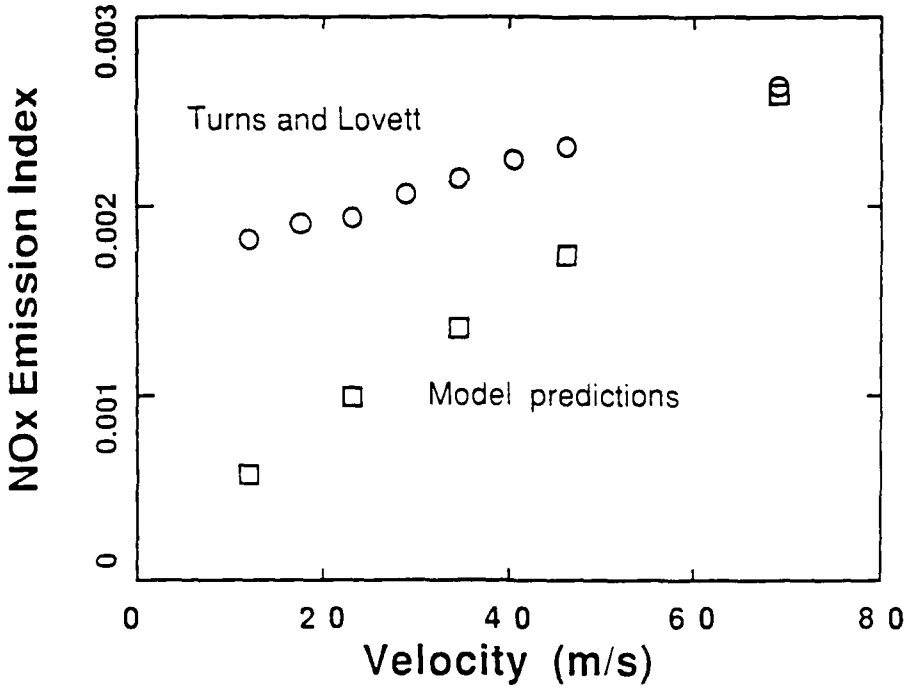

FIG. 13 Comparison of the predicted and measured emission index for a propane jet as a function of jet velocity ($d_0 = 0.386\,\text{cm}$ and $u_0 = 1.0\,\text{m/s}$).

Although, as the above results indicate, the two reactor model shows sufficient promise to justify a further extensive examination of its utility, we intend to continue, as planned, the incorporation of a more realistic treatment of the strained-flame processes into the model. Also already underway in a more accurate treatment of radiation, with the goal of understanding more completely its influence on NO_x generation.

4. Computational effort

Progress has been made in two computational efforts, partly supported under this Grant. These have yielded results which will be briefly described below.

4.1 Compressible flows

A brief description of the newly developed method for dealing with compressible flows appears in our previous report (Dimotakis *et al.* 1989a, Sec. 4.1). The first submission describing this work has been accepted and will be presented at the up-coming *AIAA Aerospace Sciences Meeting* (Lappas *et al.* 1991). Extracting from the abstract of that paper, the new method allows the computation of unsteady compressible flows, with and without chemical reactions. Viscous effects can also be included, if warranted. This work has focused on the accurate computation of the discontinuous waves that arise in such flows. The main feature of the method is the use of an adaptive Lagrangian grid. This allows the computation of discontinuous waves and their interactions with the accuracy of front-tracking algorithms. This is done without the use of additional grid points representing shocks, in contrast to how it is usually done in front-tracking schemes. The Lagrangian character of the present scheme also allows contact discontinuities to be captured easily. The algorithm derives much of its power by avoiding interpolation across discontinuities in a natural and efficient way. This results in an increased accuracy near discontinuous waves. The method has been used on a variety of reacting and non-reacting flows in order to test its ability to compute accurately, and in a robust way, complicated wave interactions. This first publication reports on progress with one-dimensional, viscous or inviscid problems.

At this writing, the method is being extended to unsteady, compressible flow in two dimensions, where local curvature of gasdynamic discontinuities can produce vorticity. This becomes an important mechanism by which compressible turbulence can differ from its incompressible counterpart.

4.2 Progress in vortex methods

The second effort involves the improvement of the computational efficiency of vortex methods, with an attendant reduction from the typical effort of order N^2, where N is the number of vortex elements, to order $N \log N$, or order N (see Dimotakis *et al.* 1989a, Sec. 4.2). Progress has also been made in the manner in which viscous, *i.e.* Reynolds number, effects are accounted for and incorporated in such calculations.

A first application and demonstration of the utility of the new methodology has been made in the investigation of Reynolds number effects in the two-dimensional, unsteady separation from an impulsively started cylinder, starting from rest. They extend to beyond the largest Reynolds numbers that have been investigated computationally to date.

We should also note, in view of the new generation of parallel computers that are making their mark, that the new method is particularly well suited for parallel computing machines. The computations were performed on the concurrent machines available at Caltech.

This work has been documented in the recently completed thesis by F. Pepin (1990), *Simulation of the Flow Past an Impulsively Started Cylinder*. Copies are available on application.

4.3 Delta machine

This part of the effort will receive a considerable boost from developments in computing resources that will be available at Caltech in the Spring of 1991. At that time the Delta machine, the largest computer in the world will be installed, built by Intel, under license from Caltech. It will be a massively parallel machine, consisting of 530 nodes, capable of 10 MFlops with 16 MBytes of memory each. The aggregate CPU power, depending on the problem, will be something like $\times 10$ to $\times 30$ the largest CRAY.

5. Diagnostics, Instrumentation & Experimental Technology

Several areas in diagnostics, instrumentation and experimental technology saw developments during the period of this Grant. Progress in the last year included the solution of an important general problem in the control of blow-down facilities and progress in digital image acquisition. These will be briefly described below.

5.1 Throttling valve control of the supersonic shear layer facility

As noted in our previous report, the supersonic shear layer facility was made possible, in large measure, by the solution of an important problem. Namely, the control of short duration, high pressure flows, potentially also at high temperature. This was accomplished by the use of a computer-controlled, rotary throttling valve, designed and fabricated at Caltech.

The rotary throttling valve is located in the high speed gas line, between the high speed side plenum and the high pressure tank. Its main purpose is to compensate for the pressure drop in the tank during the blow-down run. It works as a sonic orifice with variable cross-section and is driven by a computer- commanded, digitally-controlled dc-motor. The input signal for the motor is generated by a special interface, which was designed and built by D. Lang at GALCIT. It is, in turn, controlled by a DEC PDP-11/73 CPU based computer. The low level data acquisition and motor command routines were written by P. Dimotakis, in collaboration with D. Lang. The high level control programs were written by H. Rosemann, in collaboration with P. Dimotakis and D. Lang. The supersonic shear layer experiments in progress are part of the Ph.D. research effort of J. Hall (see Sec. 2.1).

To close the control loop, the pressures in the tank, at a station in the pipe downstream of the throttling valve, and the plenum are measured, through a 4-channel, 16-bit, 100 kHz A/D converter by the computer. The procedure to determine the valve position is slightly different for the start-up and for the usable test run time.

After the start-up procedure has allowed the pressure to reach approximately the correct level in the plenum, an estimated valve position is computed from the mass flux through the nozzle and the tank pressure, assuming choked flow in the nozzle as well as in the valve. Because the effective open area of the valve differs somewhat from the geometric one, an additional coefficient is applied. This brings the plenum pressure close to the requested value. A proportional-integral-derivative (PID) control algorithm is used to further reduce the remaining difference. Digital filters are applied to all input signals in real-time to lower the noise level.

The purpose of the start-up is to lead the system to its operating point as fast as possible to save gas, and to do that in the smoothest way possible. The first is an important

consideration, in that how well this is done sets the limits to what can be investigated during that portion of the run corresponding to uniform, controlled flow conditions. Since the whole system was designed for a total run time of the order of three seconds, or so, it is imperative that the flow starts in a second, or less. The reason for the latter is that, because the real system is highly nonlinear, the PID-control with constant gains works satisfactorily for only small deviations from the operating point. During start-up, the estimated valve position is derived from a first order linear model of the system, which accounts for the charging terms. The gain for the integration term of the control is set to zero and the other gains as well as the desired plenum pressure are increased from zero to their steady state values following a cubic (spline) fit. This provides a smooth transition to a constant plenum pressure without steps in the functions and their first and second derivatives.

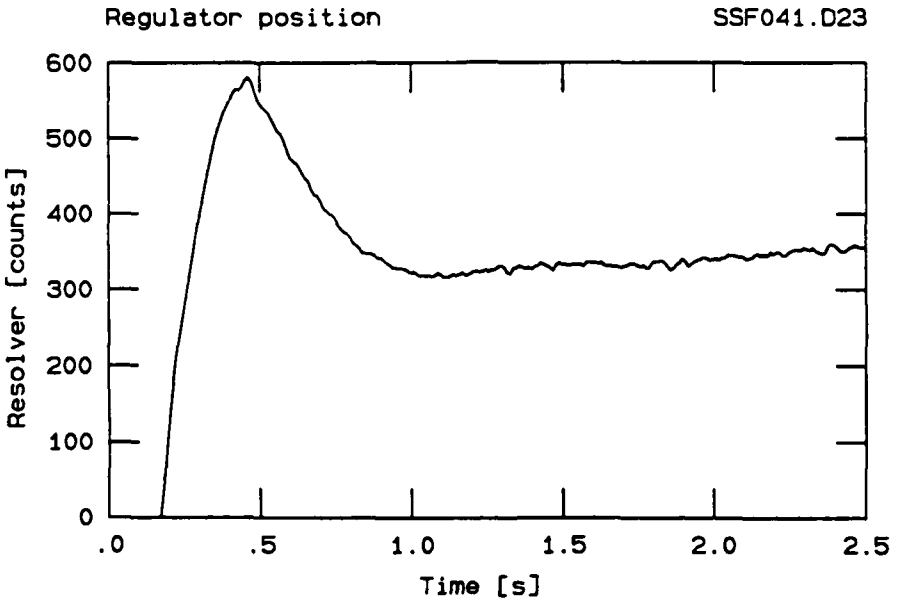

FIG. 14a Throttling valve position. Test gas: N_2.

The control program is capable of updating the valve position with a rate of at least 200 Hz, which is fully sufficient not only for the purposes of controlling the plenum pressure, but also for partially, actively damping low frequency flow instabilities in the flow supply sections.

The first tests were carried out with a reduced nozzle area to increase the time constant of the system and limit the amount of gas used. After fine-tuning the control gains and time constants with the real nozzle ($M = 1.5$) we obtained the results shown in Fig. 14a. This shows a time trace of the valve position, where about 90 valve shaft resolver counts translate into 1° angular deflection. The whole control takes place in a range of only a few shaft degrees. The curve for the plenum pressure is given in Fig. 14b. Note that, although

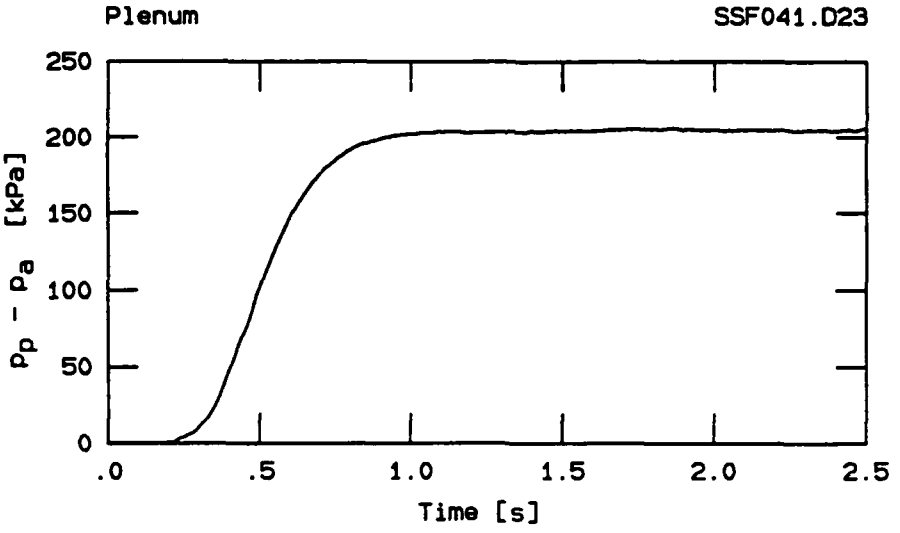

FIG. 14b Plenum pressure trace. Test gas: N_2.

the valve position shows a large overshoot, as commanded by the control algorithm, the transition of the pressure from zero to its final value is very smooth. The slow opening of teh valve, following the start-up transient, is commanded to compensate for the drop in the supply pressure, as the gas is being expended. After the start-up, the total pressure is found to be held constant to within 1%.

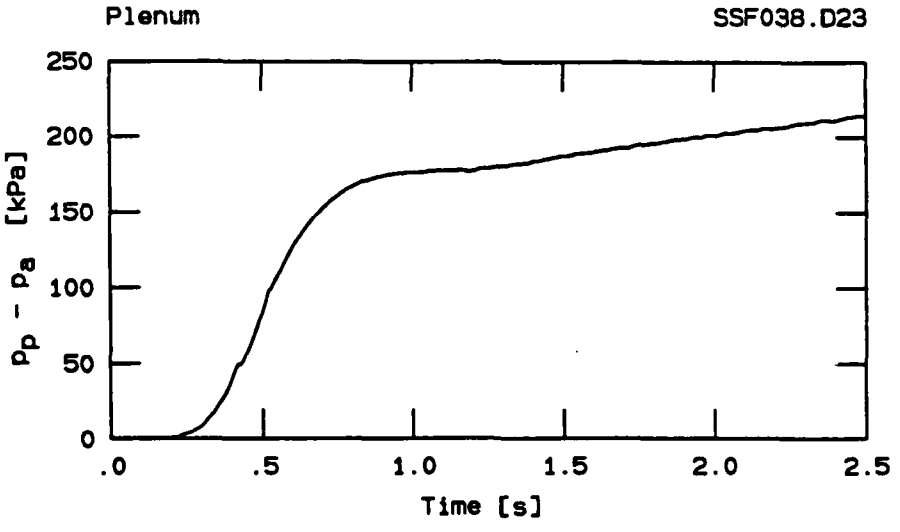

FIG. 15 Variable plenum pressure. Test gas: N_2.

The control program is not limited on keeping the pressure constant. As shown in Fig. 15, the plenum pressure can be ramped up or down at a constant rate, for example, during the run. Taking a series of Schlieren pictures and continuous pressure and temperature

measurements, pressures corresponding from underexpanded to overexpanded supersonic flow for the shear layer high speed stream can be investigated in a single run.

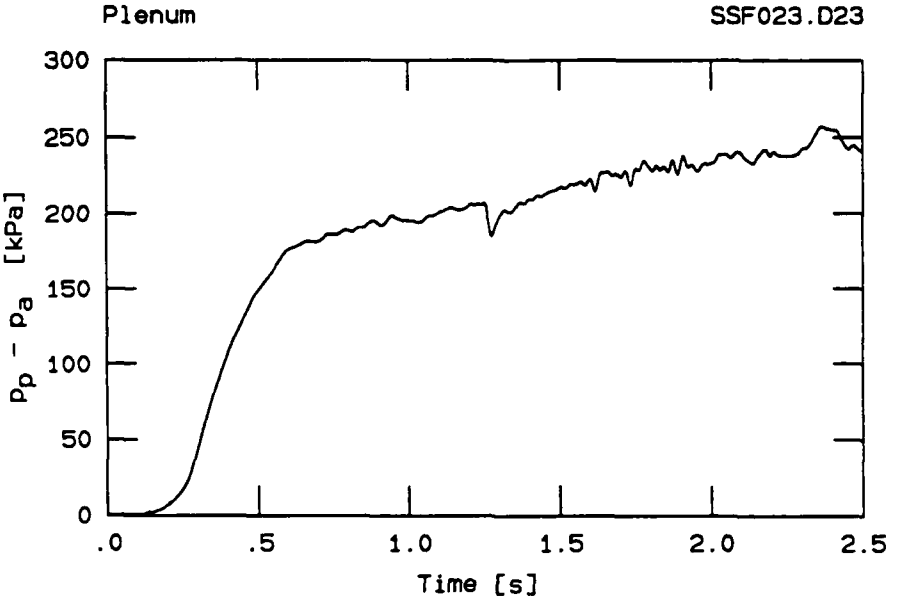

FIG. 16 Variable plenum pressure. Test gas: He.

The results in Figs. 14 and 15 were obtained with nitrogen. Because the velocity of sound in helium is much higher than in nitrogen, changing to helium effects the time constants of the system considerably. After adjusting the control constants, a reasonable control could be achieved, although not quite as good as with nitrogen, see Fig. 16.

5.2 High resolution and dynamic range digital image acquisition

A high resolution CCD-camera system purchased from Photometrics was delivered last spring. Its main component is the cryogenicaly cooled camera head containing a 1024×1024 pixel CCD focal plane array. The camera electronics include a 14-bit A/D converter. The system yields a low noise, high resolution output signal at the cost of read-out time, which is about 20 s for a full frame.

The camera system has been interfaced to DEC VAXstation 3200 and 3100 workstations, via an IEEE-488 bus. All camera functions can be controlled through this bus by the computer. While some basic image processing operations can be done in the camera system itself, most image processing is carried out on the VAXstation using a commercial program package called PV$\sim$WAVE from Precision Visuals.

The camera system will be used in an attempt to obtain cross-sectional laser Rayleigh scattering images in the Supersonic Shear Layer Facility. Single and double exposure techniques with image shifting will be applied. Currently, the system is being tested out in a water tank using a light-sheet with laser-induced fluorescence in an axisymmetric jet.

This part of the effort is being carried out by H. Rosemann, in collaboration with P. Miller, D. Lang and P. Dimotakis.

6. Personnel

In addition to the Principal Investigators:

P. E. Dimotakis: Professor, Aeronautics & Applied Physics;

J. E. Broadwell: Senior Scientist, Aeronautics;

A. Leonard: Professor, Aeronautics;

other personnel who have participated directly in the effort during the current reporting period are listed below:

E. Dahl: Member of the technical Staff, Aeronautics;

C. E. Frieler: Graduate Research Assistant, Aeronautics[‡];

R. J. Gilbrech: Graduate Research Assistant, Aeronautics;

J. L. Hall: Graduate Research Assistant, Aeronautics;

D. B. Lang: Staff Engineer, Aeronautics;

T. Lappas: Graduate Research Assistant, Aeronautics;

T. Kubota: Professor, Aeronautics;

P. L. Miller: Graduate Research Assistant, Applied Physics;

F. Pepin: Graduate Research Assistant, Aeronautics[♯];

H. Rosemann: Post-doctoral Research Fellow, Aeronautics;

M. Zhuang: Graduate Research Assistant, Aeronautics[*];

---

‡ Presently on leave to TRW Systems Group, Redondo Beach, CA.

♯ Ph.D., June 1990.

* Ph.D., June 1990, presently Post-Doctoral Research Fellow at the U. Michigan.

7. References

BARLOW, R.S., DIBBLE, R.W., LUCHT, R.P. and CHEN, J.Y. [1990] *Comb. & Flame* , in press.

BECKER, H. A. and YAMAZAKI, S. [1978] "Entrainment, Momentum and Temperature in Vertical Free Turbulent Difusion Flames", *Comb. & Flame* **33**, 123-149.

BILGER, R. W. [1979] "Turbulent Jet Diffusion Flames", *En. & Comb. Science* (Student Ed. 1, N. Chigier, ed.), 109–131.

BILGER. R. W. and BECK, R. E. [1974] "Further experiments on turbulent jet diffusion flames", *Fifteenth Symposium (International) on Combustion* (The Combustion Institute), 541.

BROADWELL, J. E. [1987] "A Model for Reactions in Turbulent Jets: Effects of Reynolds, Schmidt, and Damköhler Numbers", US-France Workshop on Turbulent Reactive Flows (Rouen, France), 7–10 July 1987. Published: *Turbulent Reactive Flows*, (eds. R. Borghi and S. N. B. Murthy, *Lecture Notes in Engineering* **40**, Springer-Verlag, 1989), 257–277.

BROADWELL, J. E. and BREIDENTHAL, R. E. [1982] "A Simple Model of Mixing and Chemical Reaction in a Turbulent Shear Layer", *J. Fluid Mech.* **125**, 397–410.

BROADWELL, J. E. and MUNGAL, M. G. [1988] "Molecular Mixing and Chemical Reactions in Turbulent Shear Layers", *22nd Symposium (International) on Combustion* (The Combustion Institute), 579–587.

CLEMENS, N. T., MUNGAL, M. G., BERGER, T. E. and VANDSBURGER, U. [1990] "Visualizations of the structure of the turbulent mixing layer under compressible conditions", *AIAA* 28th *Aerospace Sciences Meeting*, 8–11 January 1990 (Reno, Nevada), paper AIAA–90–0500.

DAHM, W.J.A. and BUCH, K.A. [1989b] "High Resolution Three-Dimensional (256^3) Spatio-Temporal Measurements in the Conserved Scalar Field in Turbulent Shear Flows", *University of Michigan Report* GRI–5087–260–1443–4.

DAHM, W. J. A. and DIMOTAKIS, P. E. [1987] "Measurements of Entrainment and Mixing in Turbulent Jets", *AIAA J.* **25**(9), 1216–1223.

DIMOTAKIS, P. E. [1989] "Turbulent Free Shear Layer Mixing and Combustion", Proceedings, 9th *ISABE* (Athens, Greece), 3–9 September 1989, 58–79.

D'MOTAKIS, P. E., BROADWELL, J. E. and LEONARD, A. [1989a] "Chemical Reactions

in Turbulent Mixing Flows", California Institute of Technology, AFOSR–88–0155 Annual Report for the period ending 15 April 1989 (15 October 1989).

DIMOTAKIS, P. E., LEONARD, A., MILLER, P. L. and DOWLING, D. R. [1989b] "Computation of 3-D Scalar dissipation PDF from 1-D gradient measurements in isotropic gradient fields", 42^{nd} Ann. Meeting, APS/DFD, paper BF4. *Bull. Am. Phys. Soc.* **34**(10), 2264.

DIMOTAKIS, P. E., BROADWELL, J. E. and ZUKOSKI, E. E. [1989c] "Combustion in Turbulent Jets and Buoyant Flames", GRI Grant No. 5087–260–1467 1988 Annual Report.

DOWLING, D. R. [1988] *Mixing in gas phase turbulent jets*, Ph.D. thesis, California Institute of Technology.

DOWLING, D. R. and DIMOTAKIS, P. E. [1988] "On Mixing and Structure of the Concentration Field of Turbulent Jets", Proceedings, *First National Fluid Dynamics Congress*, 25–28 July 1988 (Cincinatti, Ohio), **II**, 982–988.

DOWLING, D. R. and DIMOTAKIS, P. E. [1990] "Similarity of the concentration field of gas-phase turbulent jets", *J. Fluid Mech.* **218**, 109.

DOWLING, D. R., LANG, D. B. and DIMOTAKIS, P. E. [1988] "An Improved Laser-Rayleigh Scattering Photodetection System", *Exp. in Fluids* **7**(7), 435–440.

GURVICH, A. S. and YAGLOM, A. M. [1967] "Breakdown of Eddies and Probability Distributions for Small Scale Turbulence", *Phys. Fluids* (1967 Sup.), 59–65.

KOLMOGOROV, A. N. [1941] "The logarithmically normal law of distribution of dimensions of particles when broken into small parts", *Akad. Nauk SSSR* **31**(2), 99-101 (translated: V. Levin [1969] NASA-TT F–12,287).

KOLMOGOROV, A. N. [1962] "A refinement of previous hypotheses concerning the local structure of turbulence in a viscous incompressible fluid at high Reynolds number", *J. Fluid Mech.* **13**, 82–85.

LAPPAS, T., LEONARD, A. and DIMOTAKIS, P. E. [1991] "An Adaptive Lagrangian Method for Computing 1-D Reacting and Non-Reacting Compressible Flows", *AIAA* 29^{th} *Aerospace Sciences Meeting*, 7–10 January 1991 (Reno, Nevada).

MONIN, A. S. and YAGLOM, A. M. [1975] *Statistical Fluid Mechanics: Mechanics of Turbulence* **II** (Ed. J. Lumley, MIT Press).

MILLER, J. A. and BOWMAN, C. T. [1989] *Prog. in Energy and Combustion Science* (to appear).

MILLER, P. L. and DIMOTAKIS, P. E. [1989] "Stochastic Geometric Properties of Scalar Interfaces", *ASME Fluids Engineering Conference* (La Jolla, California), 10–12 July 1989, session on *Fractal Structures*.

MILLER, P. L. and DIMOTAKIS, P. E. [1990] "Reynolds Number Dependence of Scalar Fluctuations in a Turbulent Jet", *IUTAM Symposium on Fluid Mechanics of Stirring and Mixing* (La Jolla, California), 20–24 August 1990, Paper PB.4.

MUNGAL, M. G. and DIMOTAKIS, P. E. [1984] "Mixing and combustion with low heat release in a turbulent mixing layer", *J. Fluid Mech.* **148**, 349-382.

MUNGAL, M. G. and FRIELER, C. E. [1988] "The Effects of Damköhler Number in a Turbulent Shear Layer", *Comb. & Flame* **71**, 23–34.

MUNGAL, M. G. and HOLLINGSWORTH, D. K. [1989] "Organized motion in a very high Reynolds number jet", *Phys. Fluids* A 1(10), 1615–1623.

OBOUKHOV, A. M. [1962] "Some specific features of atmospheric turbulence", *J. Fluid Mech.* **13**, 77–81.

PAPAMOSCHOU, D. [1989] "Structure of the compressible turbulent shear layer", *AIAA* 27th *Aerospace Sciences Meeting*, 9–12 January 1989 (Reno, Nevada), AIAA Paper 89–0126.

PAPAMOSCHOU, D. and ROSHKO, A. [1988] "The Compressible Turbulent Shear Layer: An Experimental Study", *J. Fluid Mech.* **197**, 453–477.

PAPANTONIOU, D. and LIST, E.J. [1989] "Large-scale Structure in the Far-field of Buoyant Jets", *J. Fluid Mech.* **209**, 151–190.

PEPIN, F. [1990] *Simulation of the Flow Past an Impulsively Started Cylinder Using a Discreted Vortex Method*, Ph.D. thesis, California Institute of Technology.

PETERS, N. and DONNERHACK, S. [1981] "Structure and Similarity of Nitric Oxide Production in Turbulent Diffusion Flames", *18th Symposium (International) on Combustion (The Combustion Institute)*, 33–42.

SEITZMAN, J., PAUL, P., HANSON, R. and UNGUT, A. [1990] "PLIF Imaging Analysis of OH Structure in a Turbulent Nonpremixed H_2-Air Flame", *AIAA* 28th *Aerospace Sciences Meeting*, 8–11 January 1990 (Reno, Nevada), AIAA–90–0160.

SREENIVASAN, K. R. and MENEVEAU, C. [1986] "The Fractal Facets of Turbulence", *J. Fluid Mech.* **173**, 357–386.

TAM, C. K. W. [1971] "Directional acoustic radiation from a supersonic jet", *J. Fluid Mech.* **46**(4), 757–768.

TAM, C. K. W. and HU, F. Q. [1989] "The instability and acoustic wave modes of supersonic mixing layers inside a rectangular channel", *J. Fluid Mech.* **203**, 51–76.

TURNS, S. R. and LOVETT, J. A. [1989] "Measurements of Oxides of Nitrogen Emissions from Turbulent Propane Jet Diffusion Flames", *Comb. Sc. & Tech.* **66**, 233–249.

TYSON, T. J., KAU, C. J. and BROADWELL, J. E. [A Model of Turbulent Diffusion Flames and Nitric Oxide Generation. Part II] Energy & Environmental Res. Corp. (June 1982) Report.

WEDDELL, D. [1941] *Turbulent Mixing in Gas Flames*, Ph.D. thesis, Massachusetts Institute of Technology.

WESTBROOK, C. K. and PITZ, W. J. [1984] "Prediction of Laminar Flame Properties of Propane-Air Mixtures", *Dynamics of Flames and Reactive Systems* (ed. Bowen, J. R., *et al. Progress in Astronautics and Aeronautics* **95**, 1984) 211–235.

ZHUANG, M. [1990] *An Investigation of the Inviscid Spatial Instability of Compressible Mixing Layers*, Ph.D. thesis, California Institute of Technology.

ZHUANG, M., DIMOTAKIS, P. E. and KUBOTA, T. [1990] "The Effect of Walls on a Spatially Growing Supersonic Shear Layer", *Phys. Fluids* A **2**(4), 599–604 (included in this report as Appendix A).

Appendix A

ZHUANG, M., DIMOTAKIS, P. E. and KUBOTA, T. [1990] "The Effect of Walls on a Spatially Growing Supersonic Shear Layer", *Phys. Fluids* A **2**(4), 599–604.

Reprinted from

Physics of Fluids A
Fluid Dynamics

Volume 2 April 1990 Number 4

The effect of walls on a spatially growing supersonic shear layer

Mei Zhuang, Paul E. Dimotakis, and Toshi Kubota
Graduate Aeronautical Laboratories, California Institute of Technology, Pasadena, California 91125

pp. 599-604

a publication of the American Institute of Physics

The effect of walls on a spatially growing supersonic shear layer

Mei Zhuang,[a] Paul E. Dimotakis,[b] and Toshi Kubota[c]
Graduate Aeronautical Laboratories, California Institute of Technology, Pasadena, California 91125

(Received 9 August 1989; accepted 22 December 1989)

The inviscid instability, with respect to supersonic disturbances of a spatially growing plane mixing layer inside parallel flow guide walls, is investigated using linear stability analysis. For supersonic convective Mach numbers, it is found that the maximum amplification rates of the shear layers approach an asymptotic value and that this maximum amplification rate increases to its maximum value and decreases again as the distance between the walls decreases continuously. Contour plots of the pressure perturbation fields indicate that there are waves propagating outward from the shear layer along the Mach angle, and that the walls provide a feedback mechanism between the growing shear layer and this compression/expansion wave system. The streak lines of the flow confirm that the spreading rate of the shear layer is unusually small for supersonic disturbances.

I. INTRODUCTION

Lees and Lin[1] gave the general description of linear stability characteristics of compressible shear layers. The numerical results of Lessen *et al.*[2] showed that the flow is generally unstable with respect to supersonic disturbances, although the amplification rate is smaller than for subsonic disturbances. Experimental results of turbulent shear layer mixing by Papamoschou and Roshko[3,4] indicated that the normalized growth rate (unity for incompressible flow) reaches an asymptotic value for supersonic convective Mach numbers. The same qualitative behavior was found by Bogdanoff[5] in his analysis of several previous experimental investigations of supersonic shear layers. Recently, Ragab and Wu[6] and Zhuang *et al.*[7] studied the effects of shear layer Mach number, temperature ratio, velocity ratio, and temperature profile on the stability characteristics of two-dimensional (2-D) unbounded free shear layers with 2-D spatially growing disturbances. They found that there is a nearly universal dependence of the normalized maximum amplification rate on the convective Mach number, and that this amplification rate decreases continuously as the convective Mach number increases. These stability analyses, however, were carried out for unbounded flow, as opposed to the experiments that were conducted in enclosed test sections. Sandham and Reynolds[8] investigated the compressible shear layers using both linear theory and direct simulation. They showed that linear theory can be very useful in understanding the physics of free shear layers and the growth rate of the developed plane mixing layer.

The study of the compressible boundary-layer stability theory carried out by Mack[9,10] indicated that as long as there is a region of supersonic relative flow there will always be unstable modes present in the boundary layer. For a shear layer inside a rectangular channel, Tam and Hu[11] showed that the coupling between the motion of the shear layer and the acoustic modes of the channel produces new instability waves for the spatially growing mixing layers. Greenough *et al.*[12] considered the effects of the walls on a compressible confined temporal mixing layer. They showed that there were two general types of instabilities: confined Kelvin-Helmholtz modes and supersonic wall modes.

In this paper, we have studied the linear instability of a spatially growing plane shear layer inside parallel walls. The shear layer flow considered is inviscid and formed by the same gases in the two streams. The mean flow is treated as parallel. The purpose of this paper is to give a description of how the instability characteristics of the shear layer are affected by the flow guide walls and by the distance between the walls. For supersonic disturbances, the reflections of the compression/expansion waves from the walls can be seen in contour plots of the pressure perturbation fields. This feedback mechanism provided by the walls between the spatially growing supersonic shear layer and the wave system makes the flow more unstable than the corresponding free supersonic shear flow, provided the walls are not too close to the layer. Also, the flow patterns of the shear layers are obtained by calculating the streak lines of the shear layers.

II. FORMULATION

Consider a two-dimensional parallel flow of two streams. With upper stream quantities as the reference and the local layer thickness as the length scale, the general dimensionless quantity of flow field can be expressed as

$$Q(x,y,t) = \bar{Q}(y) + Q'(x,y,t), \tag{1}$$

where $\bar{Q}(y)$ is the mean flow quantity. Assume that the flow is subjected to small disturbances propagating in the x direction having the form

$$Q'(x,y,t) = q(y)\exp[i\alpha(x - ct)], \tag{2}$$

where α is a dimensionless complex wavenumber and c is a dimensionless complex wave velocity.

From the basic disturbance equations for infinite Reynolds number, the second-order differential equation for the dimensionless pressure disturbances can be derived, i.e.,

[a] Graduate student, Aeronautics.
[b] Professor, Aeronautics and Applied Physics.
[c] Professor, Aeronautics.

 0899-8213/90/040599-06$02.00

$$\pi''(y) - \left(\frac{2\overline{U}'}{\overline{U}-c} - \frac{\overline{T}'}{\overline{T}}\right)\pi'(y) - \alpha^2\left(1 - \frac{M_1^2}{\overline{T}}(\overline{U}-c)^2\right)\pi(y) = 0, \quad (3)$$

where M_1 is the upper stream Mach number and $\overline{U}$ and $\overline{T}$ are, respectively, the dimensionless mean velocity and temperature profiles described by a hyperbolic tangent profile and by the Crocco–Busemann relation.[7] The general configuration of the shear layer inside parallel walls is shown in Fig. 1. The dimensionless shear layer thickness, δ, is defined in a boundary-layer sense, i.e.,

$$|[U_1 - \overline{U}(\delta)]/U_1| < \epsilon, \quad |[\overline{U}(-\delta) - U_2]/U_2| < \epsilon, \quad (4)$$

where ϵ is taken as 0.002; $2h$ is the dimensionless distance between the walls.

In the regions of $\delta < y < h$ and $-h < y < -\delta$, the flow is effectively uniform, i.e., the mean velocity and temperature are constants, and Eq. (3) becomes

$$\pi'' - \lambda_k^2 \pi = 0, \quad (5)$$

with

$$\lambda_k^2 = \alpha^2[1 - (M_1^2/\overline{T}_k)(\overline{U}_k - c)^2], \quad (6)$$

for $k = 1,2$. The boundary conditions at the walls, i.e., $\pi'(h) = \pi'(-h) = 0$, then yield the analytic solutions in regions 1 and 2 as

$$\pi = A\cosh[\lambda_1(h-y)], \quad \pi = B\cosh[\lambda_2(h+y)], \quad (7)$$

where λ_1 and λ_2 are given by Eq. (6), and A and B are constants to be determined by matching to the inner flow region.

To find the solution inside the shear layer, we use the analytic solution in region 2 as a starting solution and integrate Eq. (3) numerically from $y = -\delta$ to $y = \delta$. The correct α is obtained, for a given $\omega = \alpha c$, by matching the numerical solution to the analytic solution at $y = \delta$ (shooting method). The Runge–Kutta method is used to integrate the equation and solve this eigenvalue problem.

The procedure for the calculations of the streak lines is the same as that used by Michalke.[13] The motion of a particle is given by

$$\frac{dx}{dt} = \epsilon_1 u'(x,y,t) + \overline{U}(y), \quad (8)$$

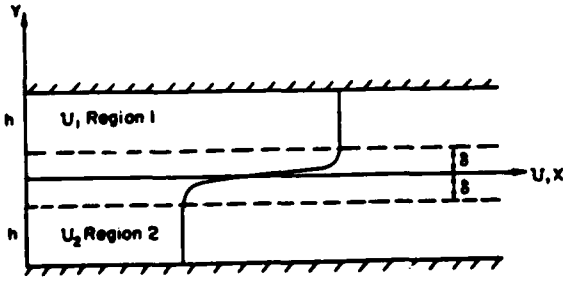

FIG. 1. The general configuration of a shear layer inside parallel walls.

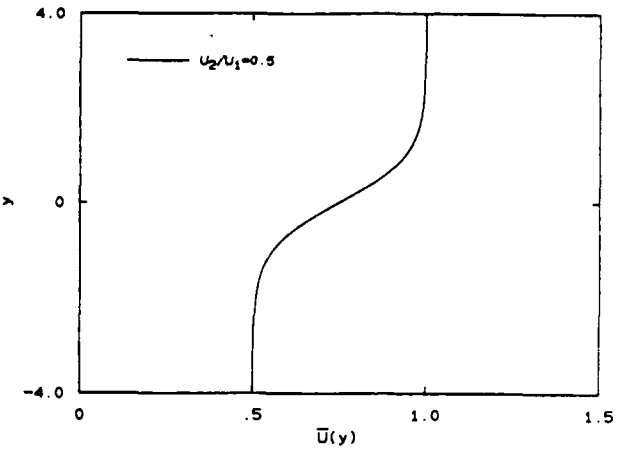

FIG. 2. Hyperbolic tangent dimensionless mean velocity profile for the velocity ratio $U_2/U_1 = 0.5$.

$$\frac{dy}{dt} = \epsilon_1 v'(x,y,t). \quad (9)$$

With appropriate initial conditions, $x(t_0) = x_0, y(t_0) = y_0$, a path line can be determined. In order to plot each streak line for a fixed time, the path lines for various initial times, t_0, are calculated. In the calculations we have chosen $x_0 = 0$, $\epsilon_1 = 0.0005$ for subsonic convective Mach numbers, and $x_0 = 0$, $\epsilon = 0.1$ for supersonic convective Mach numbers.

III. RESULTS AND DISCUSSION

The instability characteristics of shear layers with velocity and temperature profiles shown in Figs. 2 and 3 are determined for 2-D spatially growing disturbances with $h = 12$ unit lengths at different Mach numbers M_1. The main result, shown in Fig. 4, is that when the convective Mach number of the flow is supersonic, as was also noted by Mack[9,10] in his analysis of supersonic boundary-layer stability, there are

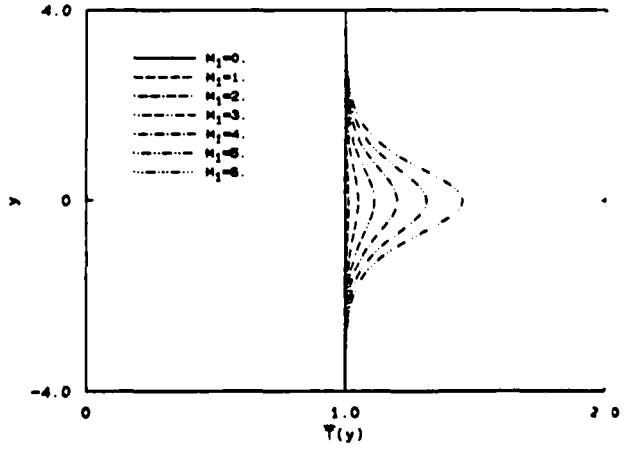

FIG. 3. Crocco–Busemann dimensionless mean temperature profiles for the case $U_2/U_1 = 0.5$ and $T_2/T_1 = 1.0$.

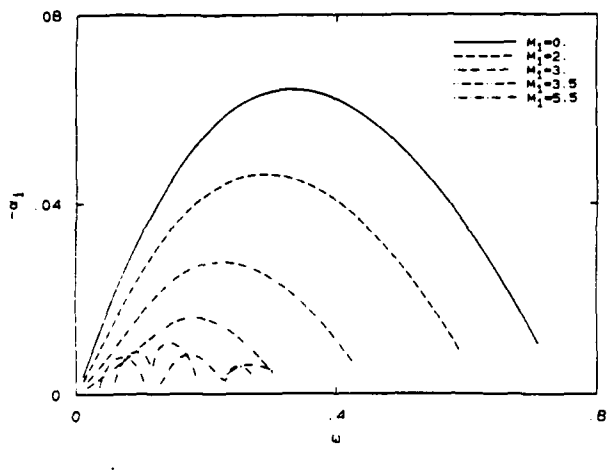

FIG. 4. Instability characteristics of the mean profiles in Figs. 2 and 3 at $h = 12$ unit lengths and $\delta = 3$ unit lengths.

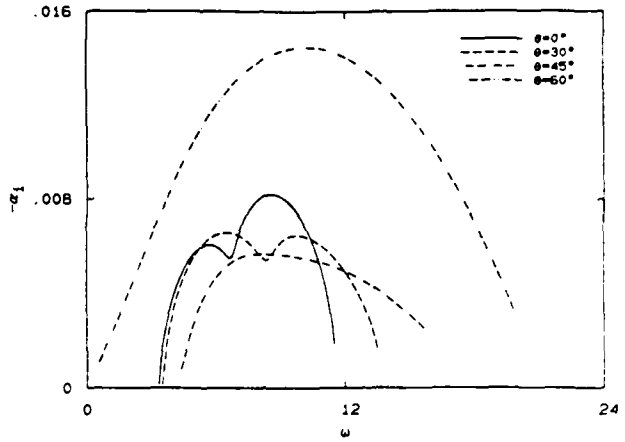

FIG. 6. Instability characteristics for 3-D spatially growing disturbances of the mean profiles at $\delta = 3$ unit lengths, $h = 20$ unit lengths, and $M_1 = 5.5$.

many supersonic unstable modes, as opposed to only one for the case of subsonic convective Mach number. The existence of many supersonic instability modes in the case of shear layers has been known from the work of Tam and Hu.[11] Their results, however, were based on the instability calculations inside a three-dimensional rectangular channel. Figure 5 (the normalized maximum amplification rate versus convective Mach number M_{c1}) indicates that the growth rate of the most unstable supersonic instability mode of shear layer with 2-D spatially growing disturbances approaches an asymptotic value as the convective Mach number becomes supersonic, which is in accord with the previously mentioned growth rate experiments.[4] The convective Mach number here is defined for each stream as[7]

$$M_{c1} = (U_1 - c_p)/a_1, \quad M_{c2} = (c_p - U_2)/a_2, \qquad (10)$$

where U_1, U_2 and a_1, a_2 are the free-stream velocities and speeds of sound, respectively, and c_p is the phase velocity of the disturbances. Alternative definitions of the convective Mach number have also been used[3,4,6,8] in which a different estimate of the convective velocity of the large structures U_c is used instead of c_p. For a 2-D mixing layer, comprised of free-stream fluids with the same ratio of specific heats, U_c is estimated by

$$U_c = (a_1 U_2 + a_2 U_1)/(a_1 + a_2). \qquad (11)$$

In our calculations, c_p is chosen to be the phase velocity of the most unstable eigenvalue. We think the definition given by Eq. (10) is more appropriate since the phase velocity of disturbances is derivable from the computations.

If a shear layer inside the parallel flow guide walls is subjected to a small 3-D spatially growing disturbance having the form

$$Q'(x,y,z,t) = q(y)\exp[i(\alpha x + \beta z - \omega t)], \qquad (12)$$

where β is a dimensionless complex wavenumber in the z direction and ω is a dimensionless real frequency, then the growth rate of the 3-D mode is larger than the corresponding 2-D mode at high convective Mach numbers over some range of propagation direction (see Fig. 6). This result shows behavior similar to the result of the previous studies of a free shear layer with 3-D spatially growing disturbances by Gropengiesser,[14] Ragab and Wu,[6] Jackson and Grosch,[15] and Sandham and Reynolds.[16] For a shear layer inside a rectangular channel, Tam and Hu[17] considered 3-D spatially growing disturbances of the form

$$p'(x,y,z,t) = \bar{p}(y)\exp[i(\alpha x - \omega t)] \times \cos(2m\pi z/B) \quad (m = 0,1,2,\ldots), \qquad (13)$$

where p' is the perturbation pressure and B is the breadth of the rectangular channel. They showed that 2-D supersonic instability waves have larger spatial growth rates than their 3-D counterparts for reasonably thick shear layers. We have conducted similar calculations of this problem, which are in agreement with the results of Tam and Hu. The instability characteristics of 3-D modes have a similar behavior as the

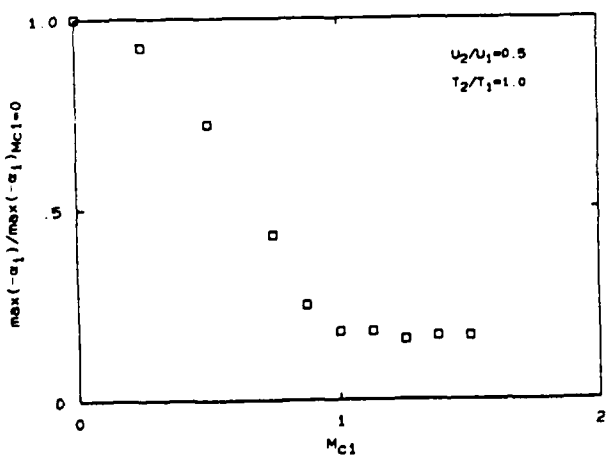

FIG. 5. Normalized maximum amplification rate versus M_{c1} at $h = 12$ unit lengths and $\delta = 3$ unit lengths.

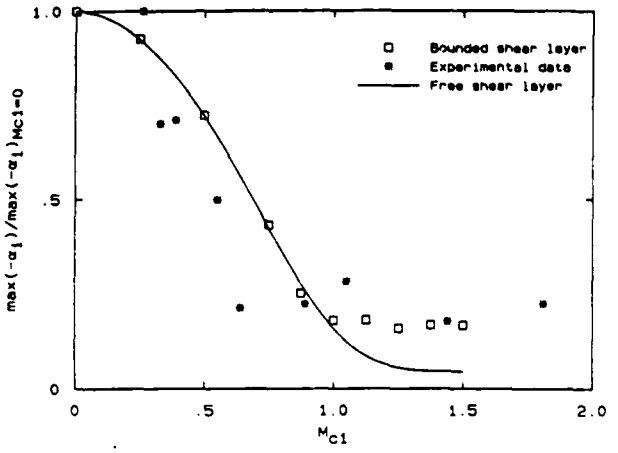

FIG. 7. A comparison of our data for a 2-D bounded shear layer with the experimental data of Papamoschou and Roshko[4] and the function $F(M_{c1})$, which was obtained by least-squares fitting the data we obtained from the previous calculations of the 2-D free shear layers.[7]

2-D modes. As a consequence, 2-D modes were considered mainly in the work described below.

Comparisons of our results shown in Fig. 5 with the experimental results of Papamoschou and Roshko,[4] and with the results obtained from the 2-D free shear layer calculations,[7] are made in Fig. 7. We can see how walls affect the instability of the shear layer. The existence of the walls makes the shear layer more unstable and keeps the maximum amplification rates from reaching an asymptotically small value for supersonic convective Mach numbers, but has no discernible effect on shear layers with subsonic convective Mach numbers.

For a fixed upper stream Mach number M_1, with the same mean velocity and temperature profiles given as described above, the instability characteristics of the shear layers with 2-D spatially growing waves are calculated at different values of h ($h = 20$, 16, 12, and 8 unit lengths). The most unstable supersonic instability mode, which is not the Kelvin–Helmholtz mode, moves to higher frequencies and its maximum amplification rate increases as the distances between the two walls decreases (see Fig. 8). But this maximum amplification rate reaches its maximum value and decreases as the distance between the walls decreases continuously (see Fig. 9). The instability characteristics of subsonic shear layers are not affected by the distance between the walls. We chose the thickness of the shear layer as the characteristic length in our calculations, which made the solution of a bounded shear layer with $h \to \infty$ approach that of the corresponding free shear layer. If we consider the distance between walls as the characteristic length, the growth rate of the supersonic instability waves scaled to this characteristic length decreases at a fixed frequency as the shear layer becomes thicker and thicker.[17]

Contour plots of the pressure perturbation fields, which combine the periodic term and the growth term, are shown in Figs. 10–13. Note that the convective Mach numbers of the shear layers corresponding to these contour plots are either close to, or over, unity, so the growth of the shear layers is small within the extent plotted. Figure 10 shows the flow with the same supersonic convective Mach numbers at both sides of the boundaries ($M_{c1} = M_{c2} = 1.375$). We can see that the compression/expansion waves propagate along the Mach angle $\mu = \arcsin(1/M_{c1})$ or $\mu = \arcsin(1/M_{c2})$ for supersonic convective Mach numbers. By measuring the Mach angle ($\mu = 45.71°$), we estimate a convective Mach number of $M_c = 1.397$, in close agreement with M_{c1} and M_{c2} estimated using Eq. (10). The variations in the strength of these compression/expansion waves suggest that these waves are reflected by the walls. Figure 11 is the contour plot for the free shear layer with the upper stream supersonic and lower stream subsonic ($M_{c1} = 1.81$ and $M_{c2} = 0.94$). The upper flow compression/expansion waves propagate with the Mach angle $\mu = 34.23°$, i.e., $M_{c1} = 1.78$, but no reflections exist. From these two contour plots we can see that for supersonic disturbances, because of the existence of the walls, the energy carried by the wave system is reflected back to the shear layer instead of being radiated to the far field.

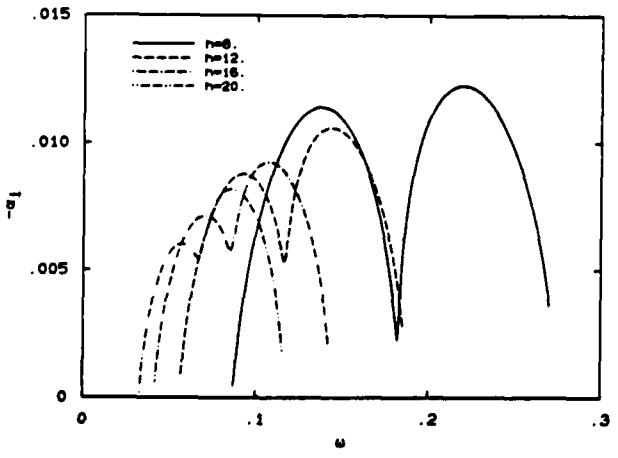

FIG. 8. Instability characteristics of the most unstable modes of the mean profiles for different values of h at $\delta = 3$ unit lengths and $M_1 = 5.5$.

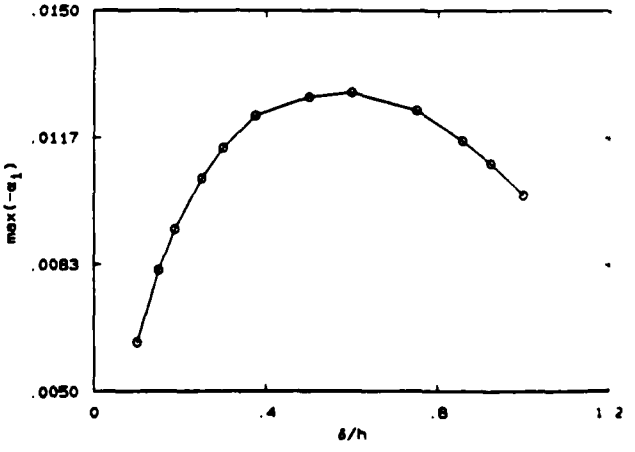

FIG. 9. The maximum amplification rate of supersonic instability mode versus δ/h at $\delta = 3$ unit lengths and $M_1 = 5.5$.

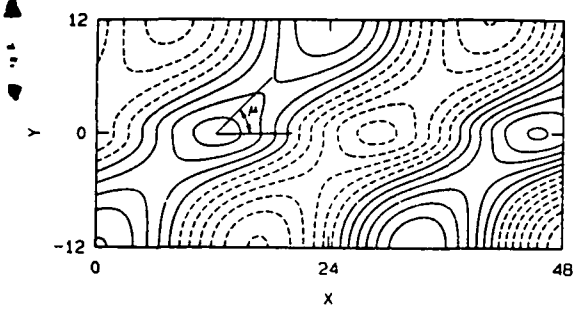

FIG. 10. Pressure pertrubation field of the most unstable mode for $\delta = 3$ unit lengths, $h = 12$ unit lengths, and $M_1 = 5.5$.

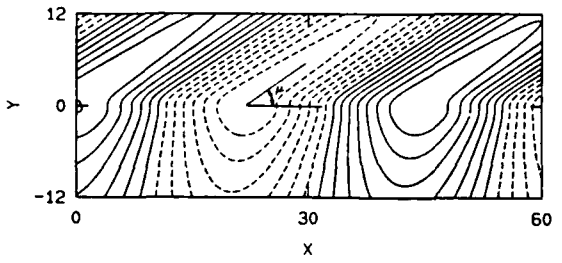

FIG. 11. Pressure perturbation field of the most unstable mode for the free shear layer at $M_1 = 5.5$.

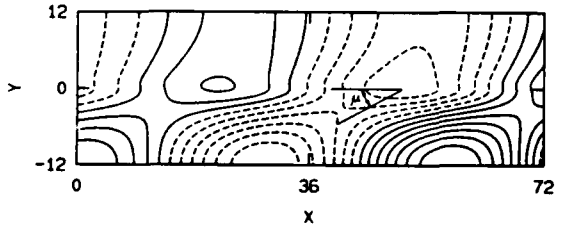

FIG. 12. Pressure perturbation field of the second unstable mode for $\delta = 3$ unit lengths, $h = 12$ unit lengths, and $M_1 = 5.5$.

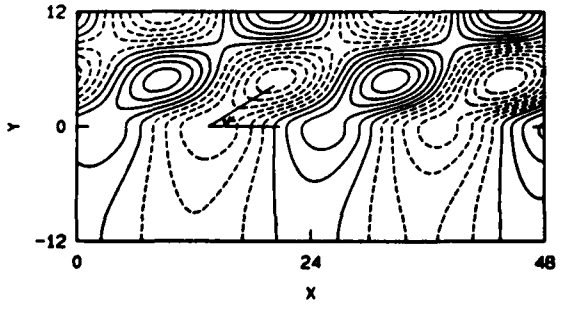

FIG. 13. Pressure perturbation field of the third unstable mode for $\delta = 3$ unit lengths, $h = 12$ unit lengths, and $M_1 = 5.5$.

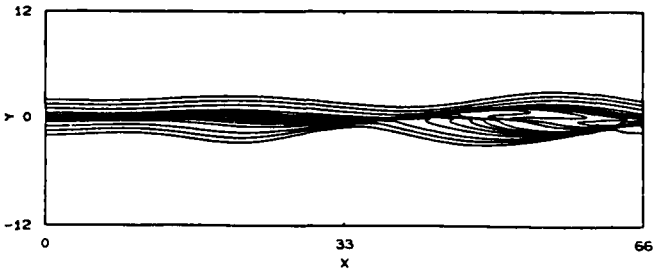

FIG. 14. Streak lines for the case $U_2/U_1 = 0.5$ and $T_2/T_1 = 1.0$ at $\delta = 3$ unit lengths, $h = 12$ unit lengths, and $M_1 = 5.5$ (supersonic convective Mach numbers $M_{c1} = M_{c2} = 1.375$).

The feedback mechanism between the growing supersonic shear layer and the wave system makes the bounded supersonic shear layer more unstable than the corresponding free supersonic shear layer, which is losing energy to acoustic radiation to the far field.[10,18] Figures 12 and 13 are two other examples of contour plots for bounded shear layers; one is with the lower stream supersonic and upper stream subsonic, and the other is vice versa. Reflections of the compression/expansion wave system propagating along Mach angles for supersonic convective Mach numbers can also be seen in those figures.

In order to describe the flow patterns of the shear layers, streak lines were also calculated for the cases of maximum amplification rates. The results plotted in Figs. 14 and 15 represent streak lines corresponding to supersonic and subsonic disturbances, respectively. These flow patterns show that, for supersonic disturbances, the growth of the shear layer, as labeled by the streak lines, is much slower than that for subsonic disturbances, and the spreading rate of the shear layer is small. The existence of the compression/expansion waves in the mixing layer with supersonic disturbances may

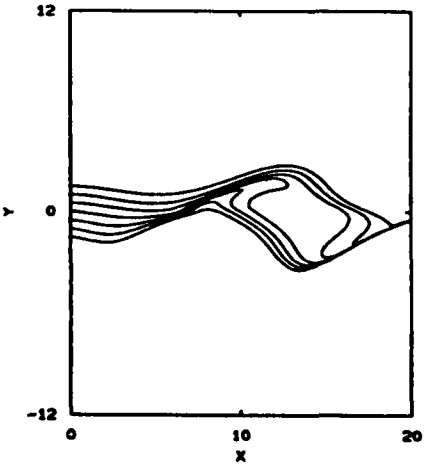

FIG. 15. Streak lines for the case $U_2/U_1 = 0.5$ and $T_2/T_1 = 1.0$ at $\delta = 3$ unit lengths, $h = 12$ unit lengths, and $M_1 = 2.0$ (subsonic convective Mach numbers $M_{c1} = M_{c2} = 0.5$).

cause the pressure gradients across the layer. Therefore the layer may be pinched by the pressure equalization.

IV. CONCLUSIONS

Spatially growing plane mixing layers inside parallel guide walls were studied using linear instability analysis. The effects of the parallel walls and the distance between them on the instability characteristics of the shear layers were investigated. The distance between such walls is found to affect the amplification rates of the characteristics of the shear layers for supersonic convective Mach numbers. As the distance decreases continuously, the maximum amplification rate of the shear layer increases to its maximum value and decreases again. For supersonic convective Mach numbers, the reflections of the compression/expansion waves caused by the parallel walls provide a feedback mechanism between the growing shear layer structures and the wave system, so the bounded shear layers are more unstable than the corresponding free shear layers. The maximum amplification rates of the bounded shear layers are found to approach an asymptotic value as the convective Mach number is increased.

ACKNOWLEDGMENT

This research was supported by the Air Force Office of Scientific Research, Grant No. AFOSR-88-0155.

[1]L. Lees and C. C. Lin, NACA Tech. Note No. 1115, 1946.
[2]M. Lessen, J. A. Fox, and H. M. Zien, J. Fluid Mech. **25**, 737 (1966).
[3]D. Papamoschou and A. Roshko, AIAA Paper No. 88-0162, 1986.
[4]D. Papamoschou and A. Roshko, J. Fluid Mech. **197**, 453 (1988).
[5]D. W. Bogdanoff, AIAA J. **21**, 926 (1983).
[6]S. A. Ragab and J. L. Wu, AIAA Paper No. 88-0038, 1988.
[7]M. Zhuang, T. Kubota, and P. E. Dimotakis, AIAA Paper No. 88-3538-CP, 1988.
[8]N. Sandham and W. Reynolds, AIAA Paper No. 89-0371, 1989.
[9]L. M. Mack, Jet Propulsion Laboratory, Document No. 900-277, Revision A, 1969.
[10]L. M. Mack, AGARD Report No. 709, 1984.
[11]C. K. W. Tam and F. Q. Hu, AIAA Paper No. 88-3675-CP, 1988.
[12]J. Greenough, J. Riley, M. Soetrisno, and D. Eberhardt, AIAA Paper No. 89-0372, 1989.
[13]A. Michalke, J. Fluid Mech. **23**, 521 (1965).
[14]H. Gropengiesser, NASA TT-F-12, 786, 1970.
[15]T. L. Jackson and C. E. Grosch, ICASE Report No. 88-33, 1988.
[16]N. Sandham and W. Reynolds, AIAA Paper No. 89-0371, 1989.
[17]C. K. W. Tam and F. Q. Hu, J. Fluid Mech. **203**, 51 (1989).
[18]P. E. Dimotakis, AIAA Paper No. 89-0262, 1989.